Draft version February 5, 2008
Preprint typeset using LaTeX style emulateapj v. 10/09/06

arXiv:astro-ph/0703456v2 5 Jul 2007

PHOTOMETRIC PROPERTIES OF THE MOST MASSIVE HIGH-REDSHIFT GALAXIES

Brant Robertson[1,2,4,5], Yuexing Li[3], Thomas J. Cox[3], Lars Hernquist[3] & Philip F. Hopkins[3]

Draft version February 5, 2008

ABSTRACT

We calculate the observable properties of the most massive high-redshift galaxies in the hierarchical formation scenario where stellar spheroid and supermassive black hole growth are fueled by gas-rich mergers. Combining high-resolution hydrodynamical simulations of the hierarchical formation of a $z \sim 6$ quasar, stellar population synthesis models, template AGN spectra, prescriptions for interstellar and intergalactic absorption, and the response of modern telescopes, the photometric evolution of galaxies destined to host $z \sim 6$ quasars are modeled at redshifts $z \sim 4 - 14$. These massive galaxies, with enormous stellar masses of $M_\star \sim 10^{11.5} - 10^{12} M_\odot$ and star formation rates of $\mathrm{SFR} \sim 10^3 - 10^4 M_\odot \mathrm{yr}^{-1}$ at $z \gtrsim 7$, satisfy a variety of photometric selection criteria based on Lyman-break techniques including V-band dropouts at $z \gtrsim 5$, i-band dropouts at $z \gtrsim 6$, and z-band dropouts at $z \gtrsim 7$. The observability of the most massive high-redshift galaxies is assessed and compared with a wide range of existing and proposed photometric surveys including SDSS, GOODS/HUDF, NOAO WDFS, UKIDSS, the IRAC Shallow Survey, Ultra-VISTA, DUNE, Pan-STARRS, LSST, and SNAP. Massive stellar spheroids descended from $z \sim 6$ quasars will likely be detected at $z \sim 4$ by existing surveys, but owing to their low number densities the discovery of quasar progenitor galaxies at $z > 7$ will likely require future surveys of large portions of the sky ($\gtrsim 0.5\%$) at wavelengths $\lambda \gtrsim 1\mu$m. The detection of rare, star-bursting, massive galaxies at redshifts $z \gtrsim 6$ would provide support for the hierarchical formation of the earliest quasars and characterize the primitive star-formation histories of the most luminous elliptical galaxies.

Subject headings: galaxies: formation – galaxies: evolution

1. INTRODUCTION

Supermassive black holes (SMBHs) serve as the relativistic engines of quasars (Lynden-Bell 1969) and the existence of quasars at $z \sim 6$ suggests the rapid formation of SMBHs with masses $M_{\rm BH} \sim 10^9 M_\odot$ (e.g., Fan et al. 2000, 2001a, 2003, 2004, 2006). Examining the consistency of rapid SMBH growth and the formation of cold dark matter (CDM) structures at high-redshifts has been of long standing theoretical interest (e.g., Efstathiou & Rees 1988), as a confluence of the deep potential well of a rare, massive dark matter halo, an abundant supply of baryons, and an efficient SMBH fueling mechanism is likely needed to grow enormous SMBHs in the available ≈ 900 Myrs before redshift $z \sim 6$. The existence of quasars at $z \sim 6$ can be considered *a posteriori* evidence that our currently dark energy-dominated (ΛCDM) universe can muster this confluence, but little else is known observationally about the associated formation of quasar host galaxies at such high redshifts. The focus of this paper is to assist in the detection and characterization of massive galaxies destined to host $z \sim 6$ quasars by calculating their photometric evolution in the scenario where ΛCDM structure formation fuels SMBHs and grows stellar spheroids through gas-rich mergers.

The formation of stellar spheroids through mergers of disk galaxies has been a long-established vehicle for galaxy evolution (e.g., Toomre & Toomre 1972; Toomre 1977). If the disk galaxies contain gas before the merger, gravitational torques can enable gas to loose angular momentum, flow efficiently to the centers of the merging systems, and result in a starburst (Larson & Tinsley 1978; Noguchi 1988; Hernquist 1989; Barnes & Hernquist 1991, 1996; Mihos & Hernquist 1994, 1996). The efficient fueling of starbursts by mergers may explain ultraluminous infrared galaxies (ULIRGS, e.g. Soifer et al. 1984; Young et al. 1986; Soifer et al. 1987; Sanders & Mirabel 1996) as an intermediate phase where the high infrared luminosities are powered by star formation before gas accretion can grow central supermassive black holes to be massive enough to become luminous quasars (Sanders et al. 1988b,a; Hernquist 1989; Sanders & Mirabel 1996; Genzel et al. 1998). This evolutionary picture would paint starbursts, ULIRGS, and quasars as stages in a structure formation process that builds spheroid and SMBH mass contemporaneously through galaxy mergers.

The observed correlations between SMBH mass and stellar spheroid mass (the $M_{\rm BH}-M_{\rm bulge}$ relation, e.g. Kormendy & Richstone 1995; Magorrian et al. 1998; Marconi et al. 2003; Häring & Rix 2004), SMBH mass and stellar velocity dispersion (the $M_{\rm BH}-\sigma$ relation, Ferrarese & Merritt 2000; Gebhardt et al. 2000; Tremaine et al. 2002), and the black hole fundamental plane (Hopkins et al. 2007a) have been widely interpreted as evidence for the coeval or coupled formation of SMBHs and stellar spheroids (e.g. Silk & Rees 1998; Fabian 1999; Kauffmann & Haehnelt 2000; Volonteri et al. 2003; Wyithe & Loeb 2003; King

[1] Kavli Institute for Cosmological Physics, and Department of Astronomy and Astrophysics, University of Chicago, 933 East 56th Street, Chicago, IL 60637, USA
[2] Enrico Fermi Institute, 5640 South Ellis Avenue, Chicago, IL 60637, USA
[3] Harvard-Smithsonian Center for Astrophysics, 60 Garden St., Cambridge, MA 02138, USA
[4] Spitzer Fellow
[5] brant@kicp.uchicago.edu

2003; Granato et al. 2004; Hopkins et al. 2006a,b). Hydrodynamical simulations of the formation of SMBHs and their host spheroids in gas-rich mergers (Di Matteo et al. 2005; Robertson et al. 2006b) that include a prescription for SMBH growth and feedback (Springel et al. 2005b) generically predict that such mergers undergo starbursts, consistent with earlier simulations that did not include SMBH modeling (e.g., Mihos & Hernquist 1994; Barnes & Hernquist 1996), and that the spheroid forms primarily before the growing SMBHs reach their final mass. Once the rapidly growing SMBHs become massive enough to drive energetic outflows, the SMBH feedback truncates star formation (Di Matteo et al. 2005; Springel et al. 2005a) and becomes visible as a luminous quasar as the outflow removes obscuring material at the galaxy center (Hopkins et al. 2005). Ultimately, the end state of this dissipative process is a spheroidal remnant that closely matches observed elliptical galaxy structural (e.g., Robertson et al. 2006a) and kinematic (e.g., Cox et al. 2006b) properties and satisfies the observed SMBH-spheroid correlations (Di Matteo et al. 2005; Robertson et al. 2006b; Hopkins et al. 2007a). The general consistency of the evolutionary sequence as detailed by these simulations with available observational data at redshifts $z \lesssim 3$ has been discussed elsewhere (e.g., Hopkins et al. 2006a,b,c).

While a developmental connection between stellar spheroids and the SMBHs they host has observational support in the nearby universe, the properties of $z \sim 6$ quasars may complicate this simple coeval picture. The Sloan Digital Sky Survey (SDSS; York et al. 2000) was used in concert with Two Micron All Sky Survey J-band imaging (2MASS; Skrutskie et al. 1997) to photometrically identify the quasar SDSS J1148+5251, spectroscopically confirmed to reside at redshift $z = 6.42$ (Fan et al. 2003). Estimates of the SMBH mass from MgII and CIV line widths for this quasar are $M_{\rm BH} \sim 2 - 6 \times 10^9$ (Willott et al. 2003; Barth et al. 2003), suggesting that the SMBH is near its Eddington limit.

Radio observations of SDSS J1148+5251 infer the presence of molecular hydrogen from CO(3-2) emission, with $M_{\rm H2} = 2.2 \times 10^{10} M_\odot$ (Walter et al. 2003). The dynamical mass for the quasar host $M_{\rm dyn} \sim 4.5 \times 10^{10} M_\odot$, estimated from CO line widths (Walter et al. 2003, 2004), suggests that the molecular gas and SMBH, rather than some dominant stellar component, supply the majority of the local potential within ~ 2.5kpc. However, radiative transfer calculations of CO line emission in quasars show that owing to projection effects the small observed line widths could be consistent with presence of a massive bulge in the quasar host galaxy, but such observed orientations are unlikely (Narayanan et al. 2006). The large IR luminosity $L_{\rm IR} \approx 10^{13} L_\odot$ (Bertoldi et al. 2003) and radio continuum imaging (Carilli et al. 2004) imply a star formation rate of $\sim 3,000 M_\odot {\rm yr}^{-1}$ if the emission is powered by reprocessed starlight, and the presence of dust and metals may suggest a prior epoch of star formation in the system (Barth et al. 2003; Walter et al. 2003; Bertoldi et al. 2003; Carilli et al. 2004). The general uncertainty about the presence of a massive stellar component in $z \sim 6$ quasars then poses two questions: if the progenitors and descendants of $z \sim 6$ quasars do contain a substantial stellar component what would their properties be and how might one detect them?

The detection of high-redshift galaxy populations at redshifts $z \gtrsim 3$ has greatly developed over the last fifteen years. The adoption of photometric techniques to identify the Lyman break in galaxy spectra (e.g., Steidel & Hamilton 1992, 1993; Steidel et al. 1996), owing to intergalactic medium (IGM) absorption (e.g., Madau 1995), the Balmer and 4000Å spectral break (e.g., Franx et al. 2003), and narrow-band searches for Lyα emission (e.g. Cowie & Hu 1998; Hu et al. 2002) has led to the discovery of galaxy populations at progressively higher redshifts. Multicolor *Hubble Space Telescope* (HST) observations of the Hubble Deep Field (HDF; Williams et al. 1996) allowed for the efficient identification of large numbers of B_{435}-band (F435W filter) dropout candidates at $3.5 \lesssim z \lesssim 4.5$ (Madau et al. 1996) and redder, more distant dropout candidates (e.g., Lanzetta et al. 1996) including a V_{606}-band (F606W filter) dropout spectroscopically verified to reside at $z = 5.34$ (Spinrad et al. 1998).

Subsequently, photometric dropout techniques based on the Lyman spectral break were used to identify high-redshift galaxy populations in the Hubble Ultra Deep Field (HUDF; Beckwith et al. 2006) with the Advanced Camera for Surveys (ACS; Ford et al. 1998) and the Near Infrared Camera and Multi-Object Spectrometer (NICMOS) Ultra Deep Field (Thompson et al. 2005), and in the wider Great Observatories Origins Deep Survey (GOODS; Dickinson et al. 2003; Giavalisco et al. 2004a). As with the HDF data, color selections based on B_{435}- and V_{606}-dropouts were used (e.g., Giavalisco et al. 2004b), but large samples based on i_{775}-band (F775W filter) and even z_{850}-band (F850LP filter) dropouts have been identified in GOODS and the HUDF by several groups (e.g., Stanway et al. 2003, 2004b,a, 2005; Yan et al. 2003, 2004; Yan & Windhorst 2004; Yan et al. 2006; Bunker et al. 2003, 2004; Bouwens et al. 2003, 2004; Bouwens & Illingworth 2006; Bremer et al. 2004; Dickinson et al. 2004; Stiavelli et al. 2004; Eyles et al. 2006; Dunlop et al. 2006; Overzier et al. 2006; Lee et al. 2006; Reddy et al. 2006; Vanzella et al. 2006; Verma et al. 2007). The GOODS optical and near-infrared data sets have been combined with *Spitzer Space Telescope* (Werner et al. 2004) observations using the Infrared Array Camera (IRAC; Fazio et al. 2004) to help constrain longer wavelength portions of the spectral energy distributions (SEDs) of high-redshift galaxy candidates (e.g., Mobasher et al. 2005; Egami et al. 2005; Yan et al. 2005; Eyles et al. 2005; Stark et al. 2006; Papovich et al. 2006; Labbé et al. 2005, 2006, see also Barmby et al. (2004)).

Parallel efforts have been made with ground-based observations, sometimes in concert with HST or *Spitzer* data sets, including optical break searches (Franx et al. 2003; Daddi et al. 2003; van Dokkum et al. 2004), $z \gtrsim 5$ Lyman-break galaxy (LBG) searches using a variety of techniques including RIz (Lehnert & Bremer 2003), $BVRiz$ (Ouchi et al. 2004), BzK_s (Grazian et al. 2006), and $zSZJHK$ (Richard et al. 2006) color selections, and very-high redshift ($z \gtrsim 5$) narrow band and spectroscopic Lyα-emitter searches (e.g., Ellis et al. 2001; Kodaira et al. 2003; Kurk et al. 2004; Santos 2004; Ouchi et al. 2005; Chary et al. 2005; Taniguchi et al.

2005; Stern et al. 2005b; Iye et al. 2006; Kashikawa et al. 2006). Collectively, these observational efforts and others have established the existence of a substantial galaxy population at $z > 5$. A brief review of the known high-redshift galaxy population can be found in Hu & Cowie (2006).

Theoretical calculations of the photometric properties of galaxies have been explored previously by hydrodynamical simulations of cosmological structure formation at redshifts $z < 3$ (Katz et al. 1992; Davé et al. 1999; Nagamine et al. 2005a,b), $z \sim 3$ (Weinberg et al. 2002; Nagamine et al. 2004, 2006), $z \gtrsim 4$ (Harford & Gnedin 2003; Finlator et al. 2006; Night et al. 2006), and $z \gtrsim 6$ (Barton et al. 2004; Davé et al. 2006), and in semi-analytic calculations (e.g., Baugh et al. 1998; Kauffmann et al. 1999; Somerville et al. 2001). These calculations show that simulated galaxies, typically with maximum star formation rates of SFR $\lesssim 100 M_{\odot}\mathrm{yr}^{-1}$, can satisfy Lyman-break color selection techniques. These simulated galaxy samples broadly agree with the observed properties of high-redshift galaxies, but given the simulated comoving volumes ($\lesssim 0.001 h^{-3}\mathrm{Gpc}^3$), the galaxies examined to date are orders of magnitudes less massive than $z \sim 6$ quasar host halos that have comoving number densities of $n \sim 1\mathrm{Gpc}^{-3}$ (Fan et al. 2003). Furthermore, these cosmological simulations have not included prescriptions for energetic feedback from SMBH growth that have been demonstrated to influence the photometric properties of elliptical remnants formed in hydrodynamical simulations of isolated disk galaxy mergers (e.g., Springel et al. 2005a).

To calculate the photometric evolution of $z \sim 6$ quasar host galaxies, we use the simulations of Li et al. (2006) that combine merger trees measured from cosmological N-body simulations of a $1h^{-3}\mathrm{Gpc}^3$ comoving volume with hydrodynamical simulations of galaxy mergers that include gas cooling, star formation and supernovae, and a prescription for feedback from growing SMBHs to track the hierarchical formation of a massive galaxy at redshifts $z \lesssim 14$. These simulations are described in detail in Li et al. (2006) and summarized in §2. The galaxy hosts a quasar at $z \sim 6.5$ that is similar in bolometric luminosity to the $z = 6.42$ quasar SDSS J1148+5251 (Fan et al. 2003). The photometric evolution of the host galaxy is modeled before, during, and after the quasar phase by applying population synthesis models, template AGN spectra, a prescription for dust attenuation and reddening, intergalactic medium absorption, and telescope responses, and is described in §3. In §4, the photometric evolution of the host galaxy is compared with a variety of optical and near-infrared photometric selection criteria from the literature. The observability of high-redshift quasar host galaxies is assessed in §5. We provide a brief discussion in §6 and summarize and conclude in §7. We adopt a flat ΛCDM cosmology with matter density $\Omega_{\mathrm{M}} = 0.3$, dark energy density $\Omega_{\Lambda} = 0.7$, baryon density $\Omega_{\mathrm{b}} = 0.04$, spectral index $n = 1$, and root-mean-squared fluctuations on $8h^{-1}$Mpc scales of $\sigma_8 = 0.9$. Unless otherwise noted, we report magnitudes on the AB scale (Oke 1974).

2. SIMULATIONS

We use the Li et al. (2006) hydrodynamical simulation of the formation of a $z \sim 6$ quasar as input for our calculation of the photometric evolution of the most massive quasar host galaxies. The simulation is described in detail by Li et al. (2006), and other specifics of the modeling can be found in Springel et al. (2005b) and Robertson et al. (2006b), but a brief summary of the simulation follows.

The rarity of $z \sim 6$ quasars requires the simulation of very large volumes to capture the high-sigma fluctuations that give rise to early-forming massive galaxies. To accomplish this, a 400^3 particle N-body simulation of a $1h^{-3}\mathrm{Gpc}^3$ volume of a cosmology consistent with the first-year results of the *Wilkinson Microwave Anisotropy Probe* (WMAP1, $\Omega_{\mathrm{M}} = 0.3$, $\Omega_{\Lambda} = 0.7$, $\Omega_{\mathrm{b}} = 0.04$, $\sigma_8 = 0.9$, Spergel et al. 2003) was performed. This simulation, with dark matter particle mass $m_{\mathrm{DM}} = 1.3 \times 10^{12} h^{-1} M_{\odot}$ and force resolution $\epsilon = 125 h^{-1}\mathrm{kpc}$, was evolved from $z \sim 30$ to $z \sim 0$. Dark matter particles bound to the most massive halo in the volume, with $M_{\mathrm{halo}} = 3.6 \times 10^{15} h^{-1} M_{\odot}$ at $z = 0$, are identified at $z \approx 6$. The Gpc^3 volume is then resimulated (Power et al. 2003; Gao et al. 2005) from $z = 69$ to $z = 0$ with 350^3 dark matter particles, with 340^3 high-resolution dark matter particles ($M_{dm} = 2.8 \times 10^8 h^{-1} M_{\odot}$, $\epsilon = 5 h^{-1}\mathrm{kpc}$) distributed in the $\sim 1.25 \times 10^{-4} h^{-3}\mathrm{Gpc}^3$ Lagrangian volume that comprised the most massive halo at $z \sim 6$ and the remaining particles properly placed throughout the rest of the Gpc^3 volume to retain the large scale tidal field.

The ΛCDM simulation is used to follow each merger in the hierarchical formation history of the halo between $z = 14.4$ and $z = 6$. The merger history is comprised of 7 major mergers (with mass ratios less than 5 : 1) between $z = 14.4$ and $z = 8.5$ contributing to the $5.4 \times 10^{12} h^{-1} M_{\odot}$ halo mass at $z \sim 6$. To model the formation of the baryonic component of the quasar host halo, each event in the merger tree is resimulated using the smoothed particle hydrodynamics (SPH) / N-body code GADGET2 (Springel 2005). The merging systems are represented with hydrodynamical models of disk galaxies (Springel et al. 2005b) with structural properties initialized according to the Mo et al. (1998) dissipational galaxy formation formalism and scaled appropriately to high-redshift following Robertson et al. (2006b). The scalings simply fold the redshift- and mass-dependent dark matter concentrations (e.g. Bullock et al. 2001) and the redshift-dependent Hubble parameter $H(z)$ through the Mo et al. (1998) formalism, resulting in smaller, more centrally concentrated disks at higher redshifts. The orbital parameters of each progenitor galaxy (see Table 1 of Li et al. (2006)) are set such that the initial separation of the galaxies is the current host halo virial radius at the time of the merger and the pericentric passage distance is half the progenitor disk scale-length $R_{\mathrm{peri}} = 0.5 R_{\mathrm{d}}$.

The merging disk galaxies range in virial mass from the initial progenitor's $M_{\mathrm{vir}} = 6.3 \times 10^{10} h^{-1} M_{\odot}$ at $z = 14.4$ to the last merging galaxy's $M_{\mathrm{vir}} = 2.08 \times 10^{12} h^{-1} M_{\odot}$. Each progenitor disk has a mass $m_{\mathrm{d}} = 0.15 M_{\mathrm{vir}}$, with gas fractions of $f_{\mathrm{gas}} = 1$ at redshifts $z \geq 10$ and $f_{\mathrm{gas}} = 0.9$ at redshifts $8 \leq z < 10$. For the numerical parameters of the progenitor galaxy models, a fixed dark matter particle mass ($M_{\mathrm{dm}} = 1.1 \times 10^7 h^{-1} M_{\odot}$) and baryonic particle mass ($M_{\mathrm{gas}} = M_{\mathrm{star}} = 2.2 \times 10^6 h^{-1} M_{\odot}$) is used. The gravitational softening for the dark matter particles

($\epsilon_{\rm dm} = 60h^{-1}$pc) is set twice as large as for the baryonic particles ($\epsilon_{\rm gas,stars} = 30h^{-1}$pc). Star formation is treated in a McKee & Ostriker (1977) multiphase picture for the interstellar medium (ISM), implemented as a numerical algorithm by Springel & Hernquist (2003). In this multiphase ISM model, dense, star-forming gas particles are treated as a collection of cold molecular clouds embedded in a tenuous phase heated by supernovae. The star-formation rate is calibrated to reproduce the Schmidt-Kennicutt Law (Schmidt 1959; Kennicutt 1998), with the star forming gas mass calculated from the cold phase density. Stellar particles are spawned probabilistically from star- forming gas particles. Each stellar population is formed with half the mass of its parent gas particle and recycles 2% of its mass as metals through supernovae (for details, see Springel & Hernquist 2003).

The Li et al. (2006) simulation includes a prescription for SMBH accretion and feedback (for details, see Springel et al. 2005b). Each simulated galaxy is initialized with a SMBH "sink" particle that is allowed to spherically accrete through a Bondi (1952) prescription. The accretion rate is determined from the gas temperature and density near the SMBH particle, and is limited to the Eddington rate. A fraction $\epsilon_r = 0.1$ of the accreted rest mass energy released as radiation and a small fraction of this radiated energy (5%) is coupled to the surrounding gas as thermal feedback. The strength of the feedback is calibrated to reproduce the local $M_{\rm BH}-\sigma$ relation in isolated mergers of disk galaxies (Di Matteo et al. 2005). The mass of the SMBH seed in each galaxy is determined by assuming a single $200M_\odot$ black hole formed in each halo at $z = 30$, in accord with expectations from Population III star formation (e.g. Abel et al. 2002; Bromm & Larson 2004; Yoshida et al. 2003, 2006), and then experienced Eddington-limited growth until its host galaxy merged into the quasar host halo. The SMBH seeds initialized in this manner range in mass from $M_{\rm BH} = 1.5 \times 10^4 h^{-1} M_\odot$ at $z = 14.4$ to $M_{\rm BH} = 8.92 \times 10^6 h^{-1} M_\odot$ at $z = 8.5$. As dynamical friction operates on the merging galaxies during the simulation, the central regions of each system eventually coalesce. Once the SMBH particles approach to within the gravitational force resolution they are merged.

2.1. *Mergers, Star Formation Rate, and Active Galactic Nuclei Luminosity*

The seven major mergers between eight galaxies occur during five redshift eras of the evolution: the first merger between two galaxies ($M_{\rm vir,1} = 5.3\times10^{10}h^{-1}M_\odot$, $M_{\rm vir,2} = 6.3 \times 10^{10}h^{-1}M_\odot$) begins at $z = 14.4$, followed by two additional mergers ($M_{\rm vir,3} = 1.5 \times 10^{11}h^{-1}M_\odot$, $M_{\rm vir,4} = 1.77 \times 10^{11}h^{-1}M_\odot$) at $13.0 > z > 10.5$, single mergers at $10.5 > z > 9.4$ ($M_{\rm vir,5} = 4.91 \times 10^{11}h^{-1}M_\odot$) and at $9.4 > z > 8.5$ ($M_{\rm vir,6} = 7.96 \times 10^{11}h^{-1}M_\odot$), and two final mergers ($M_{\rm vir,7} = 1.6 \times 10^{12}h^{-1}M_\odot$, $M_{\rm vir,8} = 2.08 \times 10^{12}h^{-1}M_\odot$) at $z \lesssim 8.5$. The fresh gas supply introduced by each merger, combined with the high density environment and violent tidal interactions, leads to peaks in the star formation rate (SFR, Fig. 1, upper panel) that temporally correlate with the merger events. The SFR peaks near the $z \sim 8.5$ mergers with SFR $> 10^4 M_\odot{\rm yr}^{-1}$, but frequently exceeds $10^3 M_\odot{\rm yr}^{-1}$ over the redshift range $8 < z < 13$.

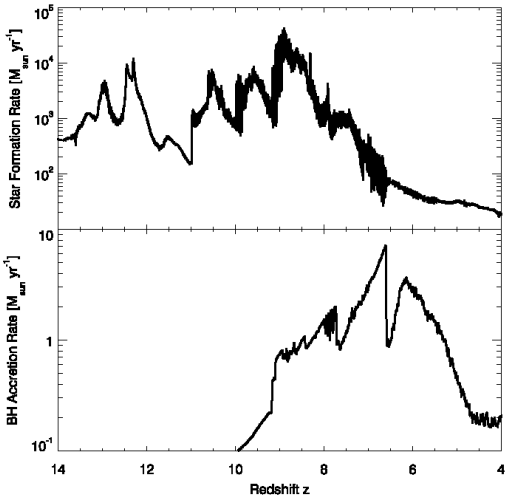

FIG. 1.— Star formation rate (SFR) and supermassive black hole (SMBH) accretion rate as a function of redshift in the Li et al. (2006) simulation of the hierarchical formation of a $z \sim 6$ quasar. The upper panel shows the SFR determined from the density of cold gas over the course of eight galaxy mergers in the build-up to quasar activity at $z \sim 6.5$. The lower panel shows the accretion rate $\dot{M}_{\rm BH}$ onto SMBHs in the system, determined through a Bondi (1952) spherical accretion model that depends on the properties of gas near the SMBH particles (for details, see Springel et al. 2005b). The unattenuated bolometric luminosity of the active galactic nuclei (AGN) fueled by SMBH accretion can be calculated from the accretion rate $\dot{M}_{\rm BH}$. Adapted from Li et al. (2006).

The total SMBH accretion rate $\dot{M}_{\rm BH}$ (Fig. 1, lower panel) also influences the observable properties of the system. The unattenuated bolometric luminosity $L_{\rm bol}$ of the active galactic nuclei (AGN) powered by the growing SMBHs is determined by the accretion rate onto the SMBHs through the equation

$$L_{\rm bol} = \epsilon_r \dot{M}_{\rm BH} c^2 = 1.45 \times 10^{12} \left(\frac{\epsilon_r}{0.1}\right) \left(\frac{\dot{M}_{\rm BH}}{M_\odot {\rm yr}^{-1}}\right) L_\odot \quad (1)$$

where $\epsilon_r = 0.1$ is the radiative efficiency of the accretion model we adopt and c is the speed of light.

3. PHOTOMETRIC MODELING

Modeling the observed spectral energy distribution (SED) of the quasar host galaxy involves calculating the SEDs of each individual stellar population and AGN present in the system and applying a wavelength-dependent dust correction to the calculated SEDs that accounts for internal interstellar absorption. The emission from the galaxy, attenuated by ISM reddening, must then be corrected for both the IGM opacity owing to Lyman series absorption and redshifting of the SED owing to cosmological expansion. The measured photometry of the object is then modified by the combined wavelength-dependent transmission of the filter and telescope assembly as well as the wavelength-dependent quantum efficiency of the detector. Below we describe how we model each contribution to the observable photometric properties of the massive quasar host galaxy.

3.1. *Stellar Population Synthesis*

The hydrodynamical simulation follows the formation of individual stellar populations formed from dense gas, as described in §2. Each stellar particle represents several million solar masses of stars, so an initial mass function (IMF) must be selected to represent distribution of stellar masses formed when each stellar particle is spawned. The IMF also influences the spectral evolution of each stellar population through its time-dependent mass-to-light ratio. We adopt the Kroupa (2001, 2002) IMF, which describes the number N of stars of a given mass m as a power-law $\mathrm{d}N/\mathrm{d}m \propto m^{-s}$. The Kroupa IMF shares the same power-law index $s \approx 2.3$ as the Salpeter (1955) IMF for $m \geq 0.5M_{\odot}$ but flattens to $s = 1.3$ at lower masses. The mass-to-light ratio of the Kroupa IMF is correspondingly lower than for the Salpeter (1955) IMF, by a factor of ~ 2, when normalized over the mass range $0.1M_{\odot} \leq m \leq 100M_{\odot}$.

The metallicity and age of each stellar particle is tracked in the simulation, allowing for the use of stellar population synthesis models to calculate an evolving SED for each particle. We use Starburst99 (Leitherer et al. 1999; Vázquez & Leitherer 2005) to model the spectra from each population, given the mass, age, metallicity, and assumed Kroupa IMF. The version of Starburst99 we use includes the Padova stellar evolution tracks (e.g., Fagotto et al. 1994) to improve the performance of Starburst99 for older ($t > 0.1$Gyr) stellar populations (for details, see Vázquez & Leitherer 2005). Illustrations of the time-dependent SEDs produced by Starburst99 can be found in Figures 4 and 5 of Vázquez & Leitherer (2005). In practice, we produce a grid of Starburst99 spectral models at wavelengths $0.0091\mu\mathrm{m} \leq \lambda \leq 160\mu\mathrm{m}$ for stellar populations over the range of ages $t = 10^4 - 10^{10}$yr, spaced logarithmically, and for metallicities of $Z = 0.02 - 2.5Z_{\odot}$, and then interpolate the Starburst99 models to produce an SED appropriate for each stellar particle.

3.2. *Active Galactic Nuclei SEDs*

As discussed in §2, the simulations follow accretion onto SMBH particles. Given the radiative efficiency we adopt ($\epsilon_r = 0.1$), we can calculate the bolometric luminosity of the AGN associated with each SMBH (Eq. 1). According to the feedback prescription by Springel et al. (2005b), a fraction $\eta = 0.05$ of this bolometric luminosity is injected as thermal energy in the surrounding gas. The remaining $\epsilon_r(1-\eta)$ fraction of the radiated energy would be visible as nuclear emission in the absence of intervening material. To model this emission, we combine the power-law + x-ray reflection component SED template for AGN from Marconi et al. (2004) with the average quasar emission template from Vanden Berk et al. (2001).

The Marconi et al. (2004) SED template consists of a power-law $L_{\nu} \propto \nu^{\alpha}$, with $\alpha = -0.44$ in the range $0.13\mu\mathrm{m} < \lambda < 1\mu\mathrm{m}$ set to match the slope inferred from stacked SDSS quasar spectra (Vanden Berk et al. 2001), and a Rayleigh-Jeans fall-off ($\alpha = 2$) at longer wavelengths. The ultraviolet ($0.05\mu\mathrm{m} < \lambda < 0.12\mu\mathrm{m}$) emission has a power-law slope ($s = -1.76$) determined by Telfer et al. (2002) based on the HST spectra of ~ 200 quasars, while the x-ray emission at energies above 1 keV is modeled with a power-law plus PEXRAV model (Magdziarz & Zdziarski 1995) reflection component. The normalization of the x-ray component relative to the optical power-law component is fixed to reproduce the quantity α_{OX} (Zamorani et al. 1981) that relates the ultraviolet ($\lambda \approx 0.25\mu$m) to x-ray ($E \approx 2$ keV) flux ratio. The Marconi et al. (2004) SED template uses a luminosity-dependent α_{OX} following Vignali et al. (2003) that leads to a decreasing fraction of the bolometric luminosity emitted in x-rays as the AGN luminosity increases. The ratio of bolometric luminosity to B-band luminosity $L_{\mathrm{bol}}/\nu_B L_{\nu,B}$ has a corresponding decrease with bolometric luminosity. Figure 3 of Marconi et al. (2004) presents illustrations of their AGN SED template and luminosity-dependent B-band and x-ray bolometric corrections.

Vanden Berk et al. (2001) produced a composite quasar spectrum by stacking the spectra of more than 2000 SDSS quasars at wavelengths $0.08\mu\mathrm{m} < \lambda < 8555\mu\mathrm{m}$, including systems with r' absolute magnitudes of $-18.0 > r' > -26.5$ over the redshift span $0.044 \leq z \leq 4.789$. The continuum of the geometric mean spectrum of these quasars can be represented by a broken power-law $L_{\nu} \propto \nu^{s}$ with $s = -0.44$ over the wavelength range $0.13\mu\mathrm{m} < \lambda < 0.5\mu\mathrm{m}$ and $s = -2.45$ at longer wavelengths, and is representative of the composite spectrum of $z \sim 6$ quasars (Fan et al. 2004). While the short wavelength slope is flatter than the slope $s \approx -0.9$ found for high-redshift quasars (Schneider et al. 1991; Fan et al. 2001b; Schneider et al. 2001), the difference can be accounted for by difficulties in determining the continuum. Prominent emission lines in the Vanden Berk et al. (2001) template spectrum include Lyα, CIV, MgII, and Hα.

To combine the Marconi et al. (2004) SED template with the Vanden Berk et al. (2001) quasar spectrum, we replace the optical power-law component of the Marconi et al. (2004) with the Vanden Berk et al. (2001) spectrum over wavelengths $0.11\mu\mathrm{m} < \lambda < 0.86\mu\mathrm{m}$ and match the Rayleigh-Jeans and UV power-law continua to the emission line spectrum. The spectrum is then integrated and renormalized to maintain the desired bolometric luminosity, and approximately maintains the emission line equivalent widths and Marconi et al. (2004) luminosity-dependent bolometric corrections while scaling the emission line flux with the AGN luminosity. As discussed below, the choice to combine these spectral templates only influences our results during the evolutionary phases when the AGN dominates the emission of the system, over small redshift ranges near $z \approx 6.5$ and $z \approx 6$ (see Fig. 1 above and Fig. 11 of Li et al. 2006), but allows us to incorporate the effect of Lyα emission on quasar color selection (e.g., Fan et al. 2001a).

3.3. *Interstellar Reddening and Absorption*

The methods for modeling the emission from stellar populations (§3.1) and AGN (§3.2) allow for an estimation of the unattenuated SEDs of simulated galaxies. The gas-rich galaxies involved in the mergers that lead to quasar activity at $z \sim 6$ contain substantial columns of hydrogen and, owing to the efficient star formation in dense gas, large amounts of obscuring dust. The wavelength-dependent attenuation from dust reddening should therefore be accounted for when modeling the observed SED of the quasar host galaxy.

To incorporate dust attenuation in the photometric modeling, the hydrogen column density N_H and an esti-

mate of the gas metallicity is calculated along the line-of-sight to each stellar population. We use the method of Hopkins et al. (2005) to calculate the gas density on a fine grid from the SPH formalism and the particle distribution. For dense gas above the threshold for star formation a two-phase decomposition of the Springel & Hernquist (2003) multiphase ISM model is performed, assuming the hot and cold phases are in pressure equilibrium, in order to calculate the hot phase column density. For each AGN in the system the column density and metallicity is measured along 100 lines-of-sight to calculate a distribution of optical depths, allowing for an estimate of the scatter in the internal galactic absorption. For discussions on general agreement between the bound-free and metal-line absorption calculated from this method for estimating N_H columns to AGN and models of the cosmic x-ray background, see, e.g., Hopkins et al. (2006a, 2007b).

Once the N_H columns and gas metallicities are calculated, the visual attenuation A_V owing to dust is calculated by scaling the Milky Way (MW) dust-to-gas ratio $A_V/N_H = 5.35 \times 10^{-22}$ (Bohlin et al. 1978; Cox 2000) by the gas metallicity. A linear scaling with metallicity, normalized to the MW ratio for solar metallicity gas, roughly accounts for the observed dust-to-gas ratios in the less metal-rich Large Magellanic Cloud (LMC) and Small Magellanic Cloud (SMC) (e.g., Fitzpatrick 1986; Rodrigues et al. 1997). The wavelength-dependent dust attenuation A_λ/A_V must also be modeled, with possible choices including the MW dust curve (e.g., Cardelli et al. 1989) that includes the strong 0.22μm absorption feature, LMC and SMC dust (e.g., Pei 1992; Gordon et al. 2003), and the possibly supernovae-related dust in high-redshift quasars (Maiolino et al. 2004). We adopt the dust model advocated by Calzetti et al. (1994) for modeling the UV emission from starburst galaxies, with the updated $R_V = 4.05$ from Calzetti et al. (2000) (see also Calzetti 1997). The Calzetti et al. (2000) dust law is frequently used to model LBGs and infer their stellar masses (e.g., Papovich et al. 2001; Shapley et al. 2005), and estimates of unattenuated star formation rates using Calzetti et al. (2000) dust corrections have been used to successfully predict the x-ray and radio properties of galaxies at $z \sim 2$ (Reddy & Steidel 2004). Using SMC dust would increase the UV absorption of the model spectra and increase the transition redshift where model spectra cross boundaries in color-color selections designed to be sensitive to the Lyman break, but would not change the photometric selection of the model spectra with a given color criterion over most of the system's redshift evolution.

3.4. *Intergalactic Medium Absorption*

Intervening hydrogen clouds in the intergalactic medium (IGM) can greatly attenuate flux via Lyman-series absorption. To account for this IGM opacity, we adopt the Madau (1995) model of Poisson-distributed absorbers in which Lyman series blanketing causes a "staircase" absorption profile blue-ward of Lyα. The spectral break introduced by this absorption has been frequently used to engineer the photometric selection of high-redshift galaxies (e.g., Madau et al. 1996; Steidel et al. 1996; Giavalisco et al. 2004b). By $z \approx 4.5$, the mean transmission is only 30% near Lyα, but the Poissonian nature of the model can lead to substantial variation in the optical depth τ at intermediate redshifts. At $z \sim 3.5$ the $\pm 1\sigma$ fluctuation in optical depth corresponds to 30% transmission variation relative to the unattenuated spectra (see, e.g., Fig. 3 of Madau 1995). However, Monte Carlo simulations suggest that the bandpass-averaged fluctuations in transmission are typically smaller (~ 0.1 magnitudes, see, e.g., Bershady et al. 1999). At high redshifts ($z \gtrsim 6$) the absorption is very strong near Lyα (e.g., $\tau > 3$, see Fig. 2 of Night et al. 2006) and typical line-of-sight fluctuations will lead to strong spectral breaks. We therefore assume the mean IGM opacity calculated from the model since we are primarily concerned with high-redshifts ($z \gtrsim 5$), but we note that the calculated photometric trajectories could experience either small shifts in color-color space position or rate of change with redshift owing to line-of-sight opacity fluctuations.

3.5. *Telescope, Filter, and Detector Response*

To calculate the observed photometric properties of simulated galaxies, the wavelength-dependent transmission of telescope assemblies, filters, and detector quantum efficiency (QE) must be modeled together to determine the net transmissivity of a given observational facility.

For the SDSS u'-, g'-, r'-, i'-, and z'-band (Fukugita et al. 1996) transmissivities, we use the USNO40 response functions measured by Jim Gunn [6]. The calculated U_n, G, and R_s (Steidel & Hamilton 1993) magnitudes use the transmissivity measured with the KPNO Mosaic CCDs [7]. For comparison with HST observations, we calculated the wavelength response curves from the combined transmissivity of the mirror and filters with the detector QE for F435W, F606W, F775W, F814W, and F850LP observations with ACS [8] and F110W and F160W observations with NICMOS [9]. For the ground-based J-, H-, and K_s-band transmissivities, we use the calculated relative response curves for 2MASS from Cohen et al. (2003). The IRAC throughput response was adopted from data provided by the Spitzer Science Center [10]. In practice, over the redshift range ($z \gtrsim 4$) considered at flux in all filters bluer than F435W were always too heavily absorbed to be easily measured (> 30 AB magnitudes), so in what follows we focus on the observable properties of galaxies in redder filters.

3.6. *Combined SED Modeling*

The final model SEDs calculated for the simulated quasar host galaxy combines the stellar population synthesis models described in §3.1, the AGN spectral template described in §3.2, ISM attenuation described in §3.3, and IGM attenuation described in §3.4, to arrive at the observed flux density (adapting the notation of Papovich et al. 2001)

$$F_\nu(z,\lambda) = (1+z)\frac{\sum_i^N L_{\nu_0,i}(\lambda_0, t_i, A_{\lambda_0,i}, M_{\star,i}, \dot{M}_{\rm BH,i})}{4\pi D_L^2(z)} \times e^{-\tau_{\rm IGM}(z,\lambda)}, \quad (2)$$

[6] http://www-star.fnal.gov/ugriz/Filters/response.html
[7] http://www.noao.edu/kpno/mosaic/filters/filters.html
[8] ftp://ftp.stsci.edu/cdbs/cdbs2/comp/acs/
[9] ftp://ftp.stsci.edu/cdbs/cdbs2/comp/nicmos/
[10] http://ssc.spitzer.caltech.edu/irac/spectral_response.html

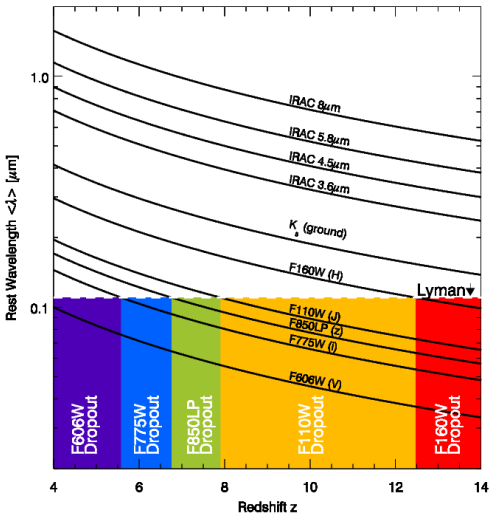

FIG. 2.— Schematic diagram of Lyα-break dropouts in optical and near-infrared filters (F606W, F775W, F850LP, F110W, F160W, K_s, 3.6μm, 4.5μm, 5.8μm, and 8.0μm) at redshifts $z \sim 4-14$. Cosmological expansion enables intergalactic medium (IGM) absorption owing to hydrogen Lyman-series opacity (e.g., Madau 1995) to absorb light at progressively longer observed wavelengths. As the Lyman-series absorption ($\sim$ 1100Å, white dashed line) shifts into redder filters, galaxies begin to drop out of the corresponding photometric samples (shaded regions represent a $> 20\%$ flux decrement in a given band for a flat spectrum). The solid lines show the effect of cosmological redshifting on the rest-frame wavelength coverage of commonly used filters.

where the rest-frame emission $L_{\nu_0,i}$ as a function of rest-wavelength λ_0 from each of N sources may depend on the its stellar age t_i, stellar mass $M_{\star,i}$, or SMBH accretion rate $\dot{M}_{\rm BH,i}$, and the dust attenuation $A_{\lambda_0,i}$ along the line-of-sight to each source. The typical number of individual stellar population sources is $N \gtrsim 750,000$ by $z \sim 6$. The total emitted spectrum from the galaxy is attenuated by the IGM optical depth τ_{IGM}, and the factors of $(1+z)$ and the luminosity distance $D_L(z)$ account for the cosmology-dependent redshift and distance. Again following Papovich et al. (2001), the flux density in each filter is calculated as

$$\langle F_\nu(z) \rangle = \frac{\int T_\nu F_\nu(z,\lambda) {\rm d}\nu/\nu}{\int T_\nu {\rm d}\nu/\nu} \quad (3)$$

where unit-free T_ν represents the combined transmissivity of the telescope and filter and the detector QE, as described in 3.5. The flux density is converted into a magnitude on the AB scale (Oke 1974) through the relation

$$m_{\rm AB} = -2.5 \log \left(\frac{\langle F_\nu \rangle}{1\mu{\rm Jy}} \right) + 23.9, \quad (4)$$

where $\langle F_\nu(z) \rangle$ is the bandpass-weighted flux density (Eq. 3) and $1\mu{\rm Jy} = 10^{-29}{\rm ergs\ cm^{-2}s^{-1}Hz^{-1}}$.

The machinery described above allows for a thorough determination of the photometric properties of a simulated galaxy and an application of common color "dropout" selection techniques based on spectral breaks to track the photometric evolution of the quasar host galaxy with redshift. For reference, a schematic diagram of the relevant redshifts for dropout samples in the ACS and NICMOS filters and a characteristic wavelength coverage for optical and near-IR filters with redshift is provided in Figure 2.

4. PHOTOMETRIC EVOLUTION

The photometric evolution of the quasar host galaxy is calculated using the methods described in §3. In our modeling, we track the luminosity of only the main host halo of the quasar during its evolution; the luminosities of the merging systems are not followed before they enter the host halo virial radius. The merging systems are modeled as almost completely gaseous, resulting in a smooth photometric evolution as each new system is added to the simulation. The variations in the system brightness owe to increases in the star formation rate during the mergers and the evolution of the combined stellar populations of the quasar host galaxy. Below, we describe the photometric evolution of the simulated system over the redshifts $z = 4-14$.

Figure 3 shows the SED and 15 magnitudes calculated for the galaxy at six characteristic times ($z \sim 12$, $z \sim 10$, $z \sim 8.5$, $z \sim 6.5$, $z \sim 5$, and $z \sim 4$) during three distinct phases in its evolution. At redshifts $z \gtrsim 7$, the system rapidly forms stars as the progenitors of the quasar host galaxy merge into the system. Each of these gas-rich mergers adds enough fuel to induce large star formation rates of SFR $\gtrsim 10^3 M_\odot {\rm yr}^{-1}$. This starburst phase coincides with the formation epoch of the stars that later form the quasar host galaxy. Over this timespan the stellar mass in the system has grown to $M_\star = 1.595 \times 10^{12} M_\odot$, or 96% of the final stellar mass at $z = 4$, with a mass-weighted mean stellar age that increases from $\langle t \rangle = 124$Myr at $z = 9$ to $\langle t \rangle = 185$Myr at $z = 7.5$. The upper panels of Figure 3 show the characteristic starburst spectrum of the galaxy during this phase, with strong rest-frame UV and blue emission. The SED evolves most strongly at long rest-frame wavelengths as the mean stellar age of the system increases, but the short wavelength rest-frame emission is remarkably similar during this phase. The luminosity of the system increases as the star formation rate and stellar mass both increase to $z \sim 8$. The large optical depth owing to Lyman-series absorption causes a near step-function break blue-ward of the Lyα line.

By $z \sim 7.5$, the quasar host galaxy begins to change rapidly. At this time a total gas mass of $M_{\rm gas} = 1.21 \times 10^{11} M_\odot$ remains, which amounts to roughly 7% of the total baryonic mass of the system. Of this gas, 30% has already been shocked, heated by feedback, or is otherwise too diffuse to form stars (e.g., Cox et al. 2006a). The remaining 5% of the star-forming baryons is dense enough to support a large star formation rate of SFR $\sim 1000 M_\odot {\rm yr}^{-1}$. However, the starburst epoch is clearly over, extinguished primarily by the consumption of the available fuel rather than by some regulatory feedback mechanism. As the star formation rate rapidly declines, the stellar population quickly ages and increases to a mean age of $\langle t \rangle = 250$Myr by $z \sim 7$ and $\langle t \rangle = 407$Myr by $z \sim 6$. While the gas supply cannot sustain the formation of a large new population of stars, it can easily support the exponential growth of SMBHs to $M_{\rm BH} \sim 10^9 M_\odot$. As the violent merging of the system continues to drive the remaining dense gas toward the galactic centers a rapid phase of

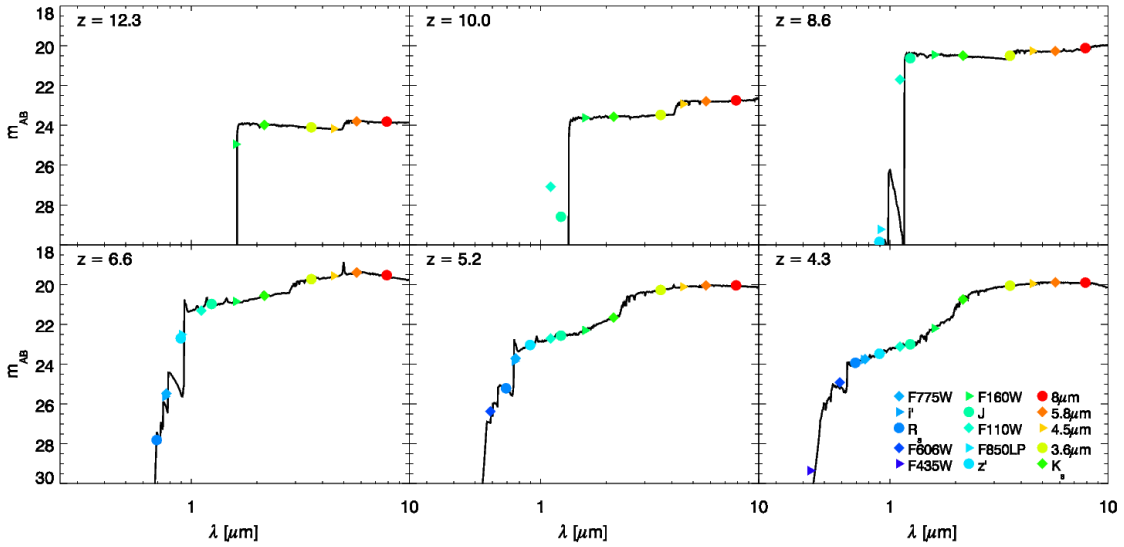

FIG. 3.— Photometric evolution of the quasar host galaxy with redshift. The spectral energy distributions (SEDs), plotted in the observed frame, are calculated from stellar and active galactic nuclei template spectra, attenuated for interstellar absorption, Lyman-series absorption in the intergalactic medium, and cosmological redshifting and distance (see §3). At early times ($z \sim 8.5 - 12$, upper panels), the galaxy is rapidly star-forming and has ultraviolet-bright rest-frame spectra typical of starburst galaxies. By $z \sim 6.5$ (bottom left panel), the SMBH accretion has peaked, leading to a luminous quasar phase that satisfies the Sloan Digital Sky Survey quasar color selection. As the SMBH accretion drops and the massive bulge ages ($z \lesssim 6$, bottom middle and right panels), the quasar host galaxy becomes a progressively redder luminous galaxy with a large Balmer/4000Å break indicative of an aging stellar population. The large bandwidth of some filters can cause an overestimate of the true flux density when they straddle the Lyα absorption line (e.g., F110W at $z \sim 10$).

Eddington-limited SMBH growth begins and eventually leads to a luminous quasar phase at $z \sim 6.5$ after the SMBHs particles coalesce. The SED of the galaxy reflects the quasar activity, with the hybrid Vanden Berk et al. (2001)-Marconi et al. (2004) model AGN spectrum dominating the blue emission of the galaxy at $z \approx 6.6$ (Fig. 3, lower left panel). The massive stellar component of the system, with a mean stellar age of $\sim$ 100s Myr, contributes substantially to the emission at rest-frame wavelengths $\lambda_0 > 0.3\mu$m and instills the SED with a Balmer/4000Å break between the K_s- and 3.6μm-bands. As feedback from the SMBH heats the gas in the central-most regions of the quasar host galaxy, the fuel source for SMBH accretion is depleted and the prominence of the AGN contribution to the SED declines. By $z \approx 5.2$ (Fig. 3, lower middle panel) the massive old stellar population with mean stellar age $\langle t \rangle = 588$Myr dominates the spectrum, with residual SMBH accretion providing less-dominant AGN activity. The rest-frame UV and blue optical portion of the SED becomes increasingly feeble compared with the observed near-IR spectral region powered by mature stars.

Below $z \sim 5$, the host galaxy continues to age and redden during its final, passive evolutionary phase. The star formation rate has declined by approximately three orders of magnitude from its peak near redshift $z \sim 9$. By $z \approx 4.3$ (Fig. 3, lower right panel) the massive stellar component has reached a mean age of $\langle t \rangle = 873$Myr, and by $z \approx 4$ the mean stellar age will increase to $\langle t \rangle = 1.01$Gyr. The UV and blue optical emission from the galaxy has correspondingly decreased, leaving a SED with a dominant Balmer/4000Å break. The SMBH accretion rate has dropped to $\dot{M}_{\rm BH} \sim 0.2 M_\odot {\rm yr}^{-1}$, bringing the bolometric luminosity of the AGN activity to $\sim 10\%$ of the bolometric luminosity of the stellar spheroid. If the system were to continue to evolve passively to low redshift, the galaxy would continue to redden. The giant spheroid would eventually become too red to appear in LBG samples, such as those defined by $U_n - G$ (Steidel & Hamilton 1993; Steidel et al. 1995) and $U_{300} - B_{450}$ (Madau et al. 1996; Steidel et al. 1996) criteria, but would be identified in Distant Red Galaxy (DRG) samples (e.g., Franx et al. 2003) with $(J - K_s) = 3.2$ and $(I - K_s) = 5.6$ (Vega) at $z \sim 3$. The quasar descendant would eventually obtain a $g' - r' = 1.24$ color (calculated assuming passive evolution to $z \sim 0.2$) typical of brightest cluster galaxies in the MaxBCG cluster catalogs of the SDSS (e.g. Koester et al. 2007).

The SEDs calculated for each of the three phases in the photometric evolution of the quasar host galaxy can be used to follow the trajectory of the system through various color-color spaces. The magnitudes calculated according the method described in §3.5 can be compared with color criteria from the literature to determine whether color-selected samples would find massive quasar host galaxies. In what follows, we examine whether the simulated galaxy satisfies common color criteria used in previous observational work. For convenience, the quasar host galaxy magnitudes in the salient observational filters at twenty redshifts $z = 14 - 4.25$ are presented in Table 1.

4.1. *V_{606}-dropout Selection*

The multi-color HST ACS observations in the GOODS fields allow for a variety of color-color selection criteria to identify LBG samples. The bluest color Lyman-break dropout techniques for HST data that overlap with the simulation redshift coverage are the V_{606}-dropout selections at $z \sim 5$. Giavalisco et al. (2004a) presented a V_{606}-dropout se-

TABLE 1
Photometric Evolution (AB Magnitudes)

Redshift	F435W	F606W	F775W	i'	z'	F850LP	F110W	F160W	K_s	$[3.6\mu m]$	$[4.5\mu m]$	$[5.8\mu m]$	$[8\mu m]$
14.00	> 30	> 30	> 30	> 30	> 30	> 30	> 30	> 30	26.11	26.27	26.39	26.40	26.40
13.18	> 30	> 30	> 30	> 30	> 30	> 30	> 30	27.77	25.68	25.81	25.89	25.65	25.57
12.32	> 30	> 30	> 30	> 30	> 30	> 30	> 30	24.94	23.97	24.09	24.16	23.80	23.81
11.04	> 30	> 30	> 30	> 30	> 30	> 30	> 30	25.08	24.70	24.60	24.25	23.83	23.83
10.03	> 30	> 30	> 30	> 30	> 30	> 30	27.08	23.61	23.56	23.47	22.92	22.79	22.74
9.600	> 30	> 30	> 30	> 30	> 30	> 30	24.01	21.67	21.75	21.96	21.59	21.61	21.61
9.209	> 30	> 30	> 30	> 30	> 30	> 30	23.83	21.98	21.98	22.03	21.57	21.57	21.48
8.555	> 30	> 30	> 30	> 30	29.85	29.22	21.69	20.45	20.49	20.49	20.25	20.26	20.11
7.970	> 30	> 30	> 30	> 30	27.92	27.84	21.93	20.92	20.92	20.30	20.08	20.05	19.97
7.467	> 30	> 30	> 30	> 30	27.14	26.00	22.35	21.49	21.41	20.40	20.28	20.20	20.12
7.008	> 30	> 30	27.74	27.45	24.58	24.04	21.96	21.32	21.12	20.07	19.96	19.81	19.80
6.607	> 30	> 30	25.62	25.47	22.69	22.50	21.31	20.84	20.55	19.72	19.56	19.39	19.52
6.467	> 30	> 30	26.69	26.55	23.74	23.57	22.38	21.84	21.51	20.18	20.06	19.99	19.94
6.300	> 30	29.90	25.81	25.71	22.95	22.87	22.09	21.66	21.31	20.15	20.00	19.90	19.91
5.993	> 30	27.99	24.94	24.75	22.24	22.22	21.89	21.58	21.21	20.16	19.96	19.87	19.94
5.563	> 30	26.68	23.91	23.76	22.57	22.55	22.24	21.96	21.48	20.25	20.06	20.00	20.02
5.007	> 30	26.22	23.80	23.69	23.21	23.19	22.87	22.40	21.58	20.23	20.10	20.03	20.02
4.491	> 30	25.28	23.68	23.65	23.37	23.35	23.02	22.26	20.91	20.07	19.98	19.91	19.93
4.250	29.51	24.99	23.79	23.77	23.49	23.47	23.12	22.22	20.77	20.06	19.96	19.89	19.90

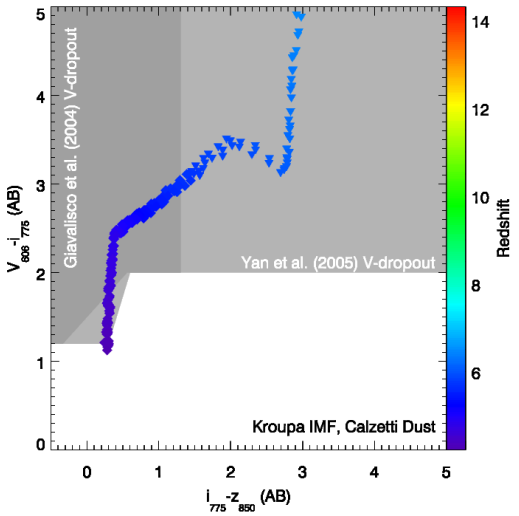

Fig. 4.— Calculated $V_{606} - i_{775}$ and $i_{775} - z_{850}$ colors with redshift for a simulated quasar host galaxy spectral energy distribution (SED). Shown is the location of the SED in this color-color space when the system SED has significant AGN activity (triangles, $5.7 \lesssim z \lesssim 6.7$) or is passively-evolving (diamonds, $z \lesssim 5.7$). Also shown are the Giavalisco et al. (2004a) GOODS and Yan et al. (2005) HUDF color selection criteria for galaxies at $z \sim 5$. The simulated galaxy satisfies these criteria during its passive evolution phase. At higher redshifts, during the epoch of AGN activity, the system will move into i_{775}-dropout samples ($i_{775} - z_{850} \gtrsim 1.3$, see Fig. 5).

lection for GOODS by the color criterion

$$\begin{gathered}\{[(V_{606} - i_{775}) > 1.5 \;\; + \;\; 0.9 \times (i_{775} - z_{850})] \\ \vee [(V_{606} - i_{775}) > \; 2.0]\} \\ \wedge \\ \{(V_{606} - i_{775}) \geq 1.2\} \\ \wedge \\ \{(i_{775} - z_{850}) \leq 1.3\}\,, \end{gathered} \tag{5}$$

where $\vee$ and $\wedge$ represent the logical "OR" and "AND" operations, and used galaxies selected in this manner to estimate the global star formation rate density at $z \sim 5$. A similar selection criterion, defined as

$$\begin{gathered}\{[(V_{606} - i_{775}) > 1.2] \wedge [(i_{775} - z_{850}) \leq 0.3]\} \\ \vee \\ \{[(V_{606} - i_{775}) > 0.4 \; + 2.67(i_{775} - z_{850})] \\ \wedge [0.3 \leq (i_{775} - \; z_{850}) \leq 0.6]\} \\ \vee \\ \{[(V_{606} - i_{775}) \geq 2.0] \wedge [(i_{775} - z_{850}) > 0.6]\}\,, \end{gathered} \tag{6}$$

was used by Yan et al. (2005) to find $z \sim 5$ galaxies in the HUDF for examination with coincident *Spitzer* IRAC observations. The application of stellar population synthesis modeling found that galaxies at $z \sim 5$ in GOODS have typical stellar masses of $M_\star \sim 10^{10} M_\odot$, stellar ages of $t \sim 1$Gyr, low extinction, and a wide range of metallicities.

Figure 4 shows the calculated $V_{606} - i_{775}$ and $i_{775} - z_{850}$ colors for the massive host galaxy at redshifts $z > 4$. The system satisfies the V_{606}-dropout color criterion over its entire passive-evolution phase at redshifts $z \lesssim 5.7$ when the SMBH accretion and star formation rates are low and the stellar component is passively aging. In V_{606}-dropout samples, the massive descendants of $z \sim 6$ quasars could appear as bright objects ($i_{775} \sim 23.5$) with red $K_s - [3.6\mu$m] colors (see Fig. 3 or Table 1). At higher redshifts ($z \gtrsim 5.7$), during an epoch of AGN activity, the system will move into i_{775}- and i'-dropout samples ($i_{775} - z_{850} \gtrsim 1.3$, see Fig. 5 and §4.2).

4.2. *i_{775}-dropout Selection*

Earlier in the evolution of the quasar host galaxy, during its phase of significant AGN activity at times $5.7 \lesssim z \lesssim 6.7$, the IGM absorption has moved into the F775W filter and the system becomes red in the $i_{775} - z_{850}$ color. To identify i_{775}-dropouts at $z \sim 6$ in the GOODS ACS data, Giavalisco et al. (2004b) and Dickinson et al. (2004) used a simple criterion given by

$$(i_{775} - z_{850}) \geq 1.3. \tag{7}$$

The GOODS data was also used to define a an i_{775}-dropout sample by Stanway et al. (2003), using similar criteria

$$\begin{gathered}\{z_{850} < 25.6\} \\ \wedge \\ \{(i_{775} - z_{850}) \geq 1.5\}\,. \end{gathered} \tag{8}$$

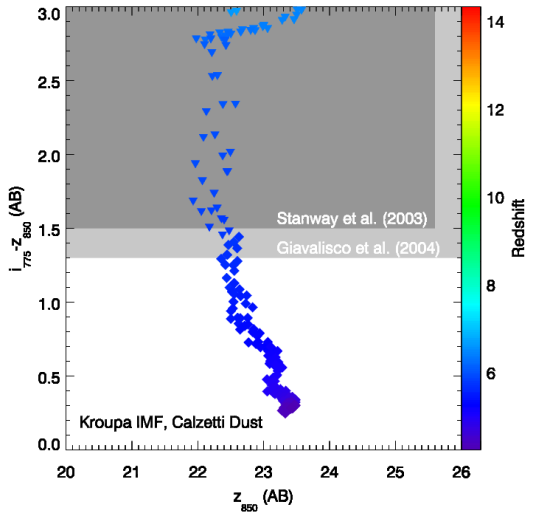

FIG. 5.— Calculated $i_{775} - z_{850}$ color and z_{850} magnitude with redshift for a simulated quasar host galaxy spectral energy distribution (SED). Shown is the location of the SED in this color-color space when the system SED is roughly starburst-dominated (circles, $z \gtrsim 6.7$), shows significant AGN activity (triangles, $5.7 \lesssim z \lesssim 6.7$) or is passively-evolving (diamonds, $z \lesssim 5.7$). Also shown are the Giavalisco et al. (2004a) and Stanway et al. (2003) GOODS color selection criteria for galaxies at $z \sim 6$. The simulated galaxy satisfies these criteria during the epoch of AGN activity and, owing to its activity and large stellar mass, is considerably brighter than the candidate $z \sim 6$ GOODS galaxies.

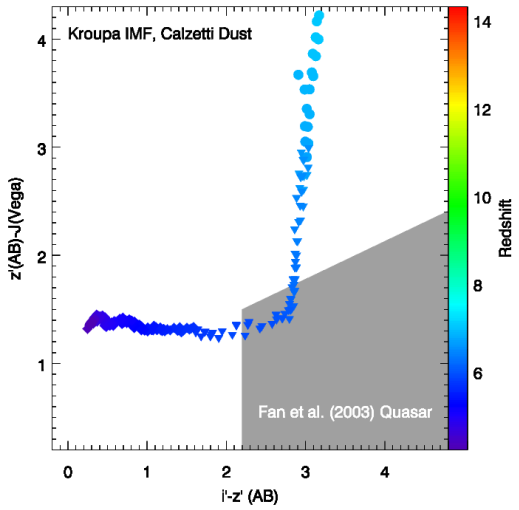

FIG. 6.— Calculated $z'_{\rm AB} - J_{\rm Vega}$ and $i'_{\rm AB} - z'_{\rm AB}$ colors with redshift for a simulated quasar host galaxy spectral energy distribution (SED). Shown is the location of the SED in this color-color space when the system SED is roughly starburst-dominated (circles, $z \gtrsim 6.7$), has significant AGN activity (triangles, $5.7 \lesssim z \lesssim 6.7$), or is passively-evolving (diamonds, $z \lesssim 5.7$). Also shown is the SDSS color selection criterion for $z \sim 6$ quasars from Fan et al. (2003). The simulated galaxy satisfies the Fan et al. (2003) color criterion during its quasar phase near $z \sim 6$ and color-selected as a SDSS quasar candidate. However, the system is ~ 2 magnitudes fainter than the $z < 20.2$ criterion used by Fan et al. (2003) to define their quasar sample.

(see also Bunker et al. 2004). Both samples were used to estimate the global star formation rate density at $z \sim 6$.

Figure 5 shows the $i_{775} - z_{850}$ color and z_{850} magnitude of the quasar host galaxy during its evolution. The simulated galaxy satisfies these criteria during its phase of AGN activity and, owing to its activity and large stellar mass ($M_\star = 1.64 \times 10^{12} M_\odot$ at $z = 6.5$), is considerably brighter ($\Delta z_{850} \sim 3$) than candidate $z \sim 6$ GOODS galaxies ($z_{850} \sim 25.5$, near the Stanway et al. (2003) magnitude cut).

4.3. *SDSS Quasar Selection*

The identification of quasars by multi-color selection criteria has been a common practice for nearly twenty years (e.g Warren et al. 1987; Irwin et al. 1991), and has proven especially fruitful for identifying distant ($z \sim 6$) quasars in the SDSS (e.g., Fan et al. 2000, 2001a, 2003, 2006). The revised selection criterion used by Fan et al. (2003), given by

$$\begin{gathered}\{z' < 20.2\} \\ \wedge \\ \{(i' - z') > 2.2\} \\ \wedge \\ \{(z' - J_{\rm Vega}) < 1.5 + 0.35(i' - z' - 2.2)\}\,, \end{gathered} \tag{9}$$

incorporates i'-dropouts determined by the SDSS data with supplemental J-band photometry to distinguish from objects with red $z' - J$ colors, such as cool stars. Figure 6 shows the $z'_{\rm AB} - J_{\rm Vega}$ and $i'_{\rm AB} - z'_{\rm AB}$ colors calculated for the quasar host galaxy over its evolution, including the phase of strong AGN activity at $z \sim 6.5$. The simulated galaxy satisfies the Fan et al. (2003) color criteria during its quasar phase near $z \sim 6.5$ and would be color-selected as a SDSS quasar candidate. However, the system is ~ 2 magnitudes fainter than the $z* < 20.2$ criterion used by Fan et al. (2003) to define their quasar sample. The quasar phase in this simulation ($z \sim 6.5$) occurs near the beginning of a broader phase of accretion and AGN activity ($7 \gtrsim z \gtrsim 5.5$), before the SMBH mass reaches its final mass. Had the peak unobscured SMBH accretion occurred slightly later (e.g., $z \sim 5.8$ rather than $z \sim 6.5$), the system would have met the magnitude cut for the Fan et al. (2003) SDSS quasar selection. We note that at $z \gtrsim 6.3$ the system moves near the L-dwarf locus in the $z' - J$ vs. $i' - z'$ color space, similar to the behavior of the quasar evolutionary track examined by Fan et al. (2003) to inform their choice of color selection criteria.

4.4. *z_{850}-dropout Selection*

The combined ACS and NICMOS observations of the HUDF and GOODS fields have allowed for a search of $z \sim 7-8$ galaxies by looking for z_{850}-dropouts. Yan & Windhorst (2004) found three z_{850}-dropout galaxies in the HUDF but concluded that their red $J_{110} - H_{160}$ colors made them unlikely to reside at $z \sim 7$. Bouwens et al. (2004) and Bouwens & Illingworth (2006) used z_{850}-dropout criteria with a blue $J_{110} - H_{160}$ color cut to find $z \sim 7$ galaxies more robustly. These color-color criteria include the selection

$$\begin{gathered}\{(z_{850} - J_{110}) > 0.8\} \\ \wedge \\ \{(z_{850} - J_{110}) > 0.8 + 0.66\,(J_{110} - H_{160})\} \\ \wedge \\ \{(J_{110} - H_{160}) < 1.2\} \end{gathered} \tag{10}$$

from Bouwens et al. (2004), the "liberal" color selection from Bouwens & Illingworth (2006)

$$\{(z_{850} - J_{110}) > 0.8\}$$

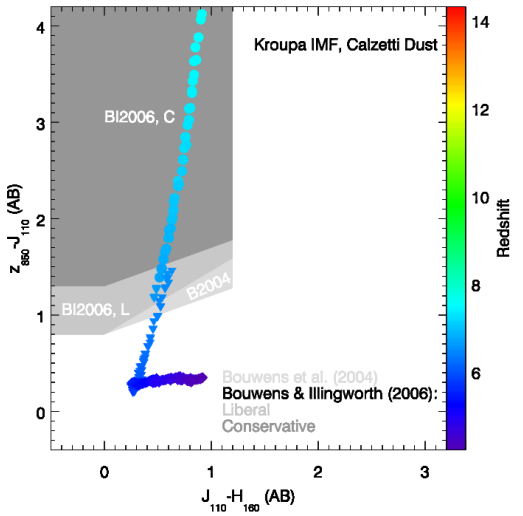

FIG. 7.— Calculated $z_{850} - J_{110}$ and $J_{110} - H_{160}$ colors with redshift for a simulated quasar host galaxy spectral energy distribution (SED). Shown is the location of the SED in this color-color space when the system SED is starburst-dominated (circles, $z \gtrsim 6.7$), shows significant AGN activity (triangles, $5.7 \lesssim z \lesssim 6.7$), or is passively-evolving (diamonds, $z < 5.7$). Also shown are the Bouwens et al. (2004) (light gray), Bouwens & Illingworth (2006)-"liberal" (gray), and Bouwens & Illingworth (2006)-"conservative" (dark gray) color selection criteria for galaxies at $z \gtrsim 7$ in NICMOS observations of the Hubble Ultra Deep Field (HUDF). The simulated $z \sim 6$ quasar host galaxy satisfies these criteria primarily during its starburst-dominated evolution phase at redshifts $z \sim 7 - 8$, but owing to its extreme star-formation rates and stellar mass it is typically ~ 6 F160W-magnitudes brighter than HUDF candidates.

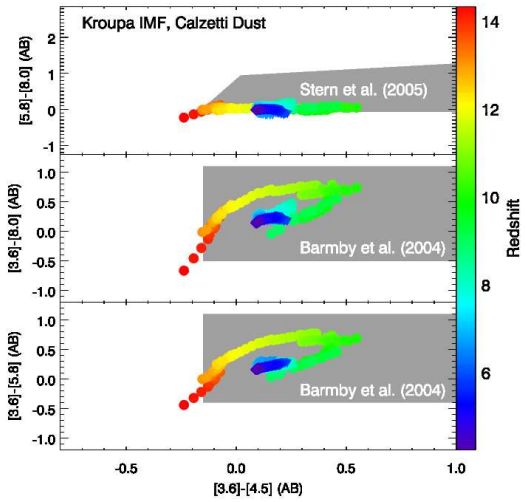

FIG. 8.— Calculated Infrared Array Camera (IRAC) colors with redshift for a simulated quasar host galaxy spectral energy distribution (SED). Shown is the location of the SED in this color-color space when the system SED is starburst-dominated (circles, $z \gtrsim 6.7$), shows significant AGN activity (triangles, $5.7 \lesssim z \lesssim 6.7$) or is passively-evolving (diamonds, $z < 5.7$). Also shown are the AGES active galaxy IR-selection from Stern et al. (2005b) and the Barmby et al. (2004) IRAC color selection criteria for LBGs at $z \sim 3$. The simulated galaxy satisfies these criteria during most of its evolution and would be detected in both the Barmby et al. (2004) IRAC observations and the IRAC Shallow Survey (Eisenhardt et al. 2004), but is $3 - 4$ AB magnitudes fainter than the AGES sub-sample of the IRAC Shallow Survey.

$$\begin{gathered} \wedge \\ \{(z_{850} - J_{110}) > 0.8 + 0.4\,(J_{110} - H_{160})\} \\ \wedge \\ \{(J_{110} - H_{160}) < 1.2\}\,, \end{gathered} \tag{11}$$

and the Bouwens & Illingworth (2006) "conservative" selection

$$\begin{gathered} \{(z_{850} - J_{110}) > 1.3\} \\ \wedge \\ \{(z_{850} - J_{110}) > 1.3 + 0.4\,(J_{110} - H_{160})\} \\ \wedge \\ \{(J_{110} - H_{160}) < 1.2\}\,. \end{gathered} \tag{12}$$

These photometric selections find < 5 high-redshift galaxies in GOODS, suggesting a rapid decline in the density of luminous star-forming galaxies and a decrease of the characteristic luminosity of galaxies by ≈ 1 AB magnitude from $z \gtrsim 6$ to $z \sim 7 - 8$.

Figure 7 shows the $z_{850} - J_{110}$ and $J_{110} - H_{160}$ colors calculated for the quasar host galaxy with redshift. The lower-redshift epochs that cover the AGN activity and passive-evolution phases occur below $z \sim 6.7$ and largely do not satisfy the z_{850}-dropout color criteria. The starburst phase at $z \gtrsim 7$, when the luminosity of the system is dominated by the young stars generated by the enormous star formation rates SFR $\sim 10^3 - 10^4$, covers the entire $z_{850} - J_{110}$ color extent of the Bouwens & Illingworth (2006) conservative selection. The starbursting quasar progenitor grows to $M_\star \approx 1.6 \times 10^{12}\,M_\odot$ in stars with a mass-weighted stellar age of $\langle t \rangle = 250$Myr at $z = 7$, powering a remarkable luminosity ~ 6 F160W-magnitudes brighter than z_{850}-dropout $z \sim 7$ candidates in GOODS. If $z \sim 6$ quasars form in the manner suggested by the Li et al. (2006) simulations, a z_{850}-dropout or similar selection criterion would be well-matched to find quasar progenitors during the peak of their spheroid formation.

4.5. *IRAC-based Selection*

In surveys at redshifts $z \lesssim 4$, the IR properties of both AGN and galaxies have been used to design color-color selection criteria using IRAC bands. Stern et al. (2005a) showed that the $[3.6\mu\text{m}] - [4.5\mu\text{m}]$ color of broad-line AGN at $1 \lesssim z \lesssim 4$ are typically redder than galaxies at $z \lesssim 2$. Their selection, given by,

$$\begin{gathered} \{([5.8\mu\text{m}] - [8.0\mu\text{m}]) > -0.07\} \\ \wedge \\ \{([3.6\mu\text{m}] - [4.5\mu\text{m}]) > -0.157 \\ +0.188\,([5.8\mu\text{m}] - [8.0\mu\text{m}])\} \\ \wedge \\ \{([3.6\mu\text{m}] - [4.5\mu\text{m}]) > -2.77 \\ +2.97\,([5.8\mu\text{m}] - [8.0\mu\text{m}])\} \end{gathered} \tag{13}$$

identified 90% of the spectroscopically identified type 1 AGN in the AGN and Galaxy Evolution Survey (AGES).

Barmby et al. (2004) used template SEDs to estimate the location of galaxies at $z \gtrsim 2$ in the $[3.6\mu\text{m}] - [5.8\mu\text{m}]$ vs. $[3.6\mu\text{m}] - [4.5\mu\text{m}]$ and $[3.6\mu\text{m}] - [8.0\mu\text{m}]$ vs. $[3.6\mu\text{m}] - [4.5\mu\text{m}]$ color-color spaces. Comparing with a sample of confirmed $z \sim 3$ LBG galaxies, they found that the majority of the

LBGs resided in the IRAC color-color regions

$$\{([3.6\mu\mathrm{m}]-[4.5\mu\mathrm{m}])>-0.15\}$$
$$\wedge$$
$$\{1.1>([3.6\mu\mathrm{m}]-[5.8\mu\mathrm{m}])>-0.4\} \quad (14)$$

and

$$\{([3.6\mu\mathrm{m}]-[4.5\mu\mathrm{m}])>-0.15\}$$
$$\wedge$$
$$\{1.1>([3.6\mu\mathrm{m}]-[8.0\mu\mathrm{m}])>-0.5\}\,. \quad (15)$$

Barmby et al. (2004) combined these criteria with selections based on R_s-band magnitude. At the redshifts we consider, the quasar host galaxy always has significant IGM attenuation of the R_s-band and is significantly redder in $R_s-[3.6\mu\mathrm{m}]$ color than the galaxies examined by Barmby et al. (2004). We therefore compare only with their IRAC color-color selections.

Figure 8 shows the calculated IRAC colors for the simulated quasar host galaxy at redshifts $z>4$. The galaxy satisfies the Barmby et al. (2004) and Stern et al. (2005b) criteria during most of its evolution. The $[3.6\mu\mathrm{m}]-[4.5\mu\mathrm{m}]$ color begins blue at redshifts $z\gtrsim 12$ when the star-forming SED has its rest-frame near-UV and optical emission in the shortest-wavelength IRAC bands. As the redshift decreases and the stellar populations age, the $[3.6\mu\mathrm{m}]-[4.5\mu\mathrm{m}]$ color increases until the Balmer/4000Å break passes through these bands and the galaxy becomes very red in $[3.6\mu\mathrm{m}]-[4.5\mu\mathrm{m}]$. At lower redshifts, the system becomes relatively stable in its $[3.6\mu\mathrm{m}]-[4.5\mu\mathrm{m}]$ color for the remainder of the simulation. The system has a consistently flat $[5.8\mu\mathrm{m}]-[8.0\mu\mathrm{m}]$ color, and would allow for its selection by the Stern et al. (2005b) criteria. However, the AGES sub-sample of the IRAC Shallow Survey (Eisenhardt et al. 2004) has a limiting magnitude ~ 3 magnitudes fainter than the complete Shallow Survey in the $[3.6\mu\mathrm{m}]$-band, and is too shallow to detect the simulated quasar host galaxy. The Barmby et al. (2004) color selections involve the $[3.6\mu\mathrm{m}]$-band and have considerably more evolution than redder bands since the $[3.6\mu\mathrm{m}]$-band transitions through the Balmer/4000Å break (see §4.6 below). The large color-color area of the Barmby et al. (2004) criterion would allow for the quasar host galaxy to be selected over almost the entire duration of the simulation (redshifts $z\lesssim 12$). All three IRAC criteria examined would be convenient methods to define color selected samples that could include quasar host galaxies at $z\gtrsim 4$.

4.6. *High-Redshift 4000Å/Balmer Breaks*

The presence of 4000Å or Balmer breaks in the observed SEDs of galaxies has been cited as evidence for evolved stellar populations in galaxies at $z\gtrsim 2$ (e.g. Franx et al. 2003). The calculated quasar progenitor star formation history (Fig. 1) suggests that a significant population of stars ($M_\star\approx 10^{11}M_\odot$) can form in such systems by $z\sim 12$. As these stars age they can contribute a small 4000Å / Balmer spectral break in the galaxy SED, as is apparent in the $z\sim 10$ SED in Figure 3, and may be detected photometrically in the near-IR.

Figure 9 shows the calculated IRAC $[3.6\mu\mathrm{m}]-[4.5\mu\mathrm{m}]$ vs. $[4.5\mu\mathrm{m}]-[5.8\mu\mathrm{m}]$ colors for the simulated quasar host galaxy at redshifts $z>4$. The observable near-IR SED is very flat over the majority of the galaxy's evolution, remaining at $([4.5\mu\mathrm{m}]-[5.8\mu\mathrm{m}])<0.2$ and $([4.5\mu\mathrm{m}]-[5.8\mu\mathrm{m}])<0.27$ at redshifts $z<9$. At higher redshifts $z\sim 9-11$ when the SED would move into J_{110}-dropout samples, the Balmer/4000Å break moves into the $[3.6\mu\mathrm{m}]$-band and causes the $[3.6\mu\mathrm{m}]-[4.5\mu\mathrm{m}]$ color to redder by $\sim 0.2-0.3$ magnitudes. As the Balmer/4000Å break moves through the

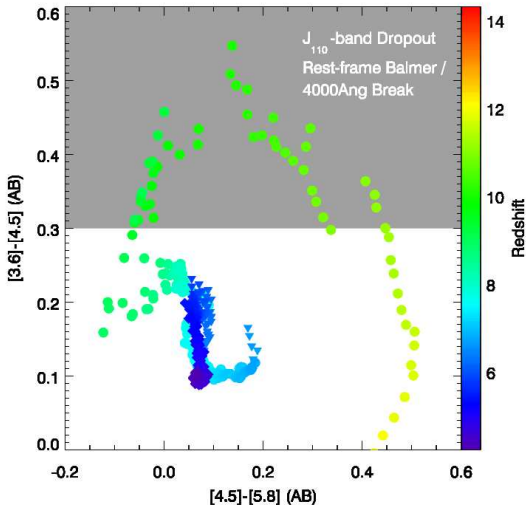

FIG. 9.— Calculated Infrared Array Camera (IRAC) $[3.6\mu\mathrm{m}]-[4.5\mu\mathrm{m}]$ vs. $[4.5\mu\mathrm{m}]-[5.8\mu\mathrm{m}]$ colors with redshift for a simulated quasar host galaxy spectral energy distribution (SED). Shown is the location of the SED in this color-color space when the system SED is starburst-dominated (circles, $z\gtrsim 6.7$), shows significant AGN activity (triangles, $5.7\lesssim z\lesssim 6.7$) or is passively-evolving (diamonds, $z<5.7$). At $z\sim 10$, the quasar progenitor has already been forming stars for $\gtrsim$ 200Myr and will display a rest-frame Balmer/4000Å spectral break. The break could be observed as a red $[3.6\mu\mathrm{m}]-[4.5\mu\mathrm{m}]$ color in J_{110}-dropout samples, analogous to the $K_s-[3.6\mu\mathrm{m}]$ spectral break measured in z_{850}-band dropouts at lower redshifts (e.g., Labbé et al. 2006).

$[4.5\mu\mathrm{m}]$-band, the evolutionary track of the SED reverses direction at higher redshifts and the system becomes substantially *bluer* in $[3.6\mu\mathrm{m}]-[4.5\mu\mathrm{m}]$ as the filters begin to probe the region of the SED sensitive to the large star formation rate (at $z\sim 12$, see the upper left panel of Fig. 3). In contrast, the trajectory of local galaxy SEDs with mature stellar populations in color-spaces sensitive to optical breaks continue to redden as the SEDs are shifted to higher redshifts (e.g., J_s-K color at redshifts $z>2.5$, see Figure 1 of Franx et al. 2003). The extremum of the $[3.6\mu\mathrm{m}]-[4.5\mu\mathrm{m}]$ at $z\sim 9-11$ owing to the rest-frame optical break makes the color a useful indicator for the presence of mature stars in J_{110}-dropout samples.

A completely analogous behavior can occur in lower redshift samples in bluer bands. SED fits to z_{850}-dropout galaxies in the HUDF at $z\sim 7$ show evidence for a rest-frame optical break in their $K-[3.6\mu\mathrm{m}]$ colors (Labbé et al. 2006), as do $z\approx 6$ galaxies (Yan et al. 2005; Eyles et al. 2005), and possibly indicate an evolved stellar component. Recently, Wiklind et al. (2007a,b) have proposed Balmer break selection criteria for post-starburst systems at $z\sim 5$ using VLT/ISAAC near-IR J, H, and K_s and IRAC $[3.6\mu\mathrm{m}]$ band observations of the GOODS fields. Their selection is defined by a union of objects in two regions: a "Region A" in the $J-K_s$ vs. $H-[3.6\mu\mathrm{m}]$ color space, given by

$$\{(J-K_s)<-1.94+3.14\,(K_s-[3.6\mu\mathrm{m}])\}$$
$$\wedge$$
$$\{(J-K_s)>-1.90+1.27\,(K_s-[3.6\mu\mathrm{m}])\}$$
$$\wedge$$
$$\{(J-K_s)>1.71-0.82\,(K_s-[3.6\mu\mathrm{m}])\}\,, \quad (16)$$

and a "Region B" in the $H-[3.6\mu\mathrm{m}]$ vs. $H-[3.6\mu\mathrm{m}]$ color

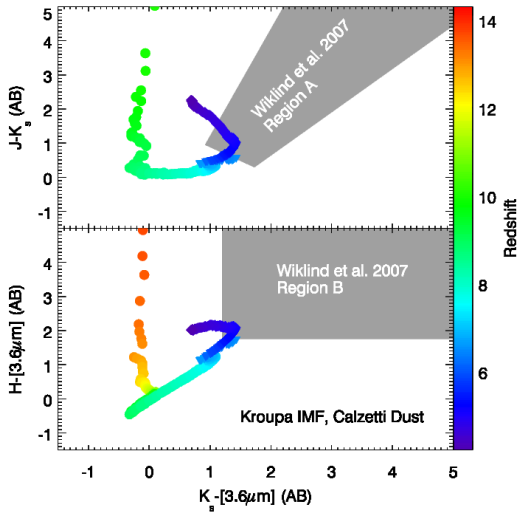

FIG. 10.— Calculated near-infrared J, H, K_s, and Infrared Array Camera (IRAC) [3.6μm] colors with redshift for a simulated quasar host galaxy spectral energy distribution (SED). Shown is the location of the SED in this color-color space when the system SED is starburst-dominated (circles, $z \gtrsim 6.7$), shows significant AGN activity (triangles, $5.7 \lesssim z \lesssim 6.7$) or is passively-evolving (diamonds, $z < 5.7$). Also shown are the "Region A" and "Region B" color selection criteria from Wiklind et al. (2007a,b) designed to identify post-starburst systems at $z \sim 5$ via the Balmer/4000$\AA$ break. The quasar descendant satisfies the Wiklind et al. (2007a,b) criteria over the redshift range $4.8 \lesssim z \lesssim 5.5$, during the post-starburst, passively-evolving phase of the system's evolution. The Wiklind et al. (2007a,b) criteria are also briefly satisfied by the galaxy at $z \sim 6.5$ during the height of the quasar activity.

space, given by

$$\{(H - [3.6\mu\mathrm{m}]) > 1.75\} \wedge \{(K_s - [3.6\mu\mathrm{m}]) > 1.20\}\,. \quad (17)$$

Figure 10 shows the calculated near-infrared J, H, K_s, and IRAC [3.6μm] colors with redshift for the quasar host galaxy SED in relation to Regions A and B from Wiklind et al. (2007a,b). The quasar descendant satisfies the Wiklind et al. (2007a,b) criteria over the redshift range $4.8 \lesssim z \lesssim 5.5$, during the post-starburst, passively-evolving phase of the system's evolution. The comparison suggests that the Wiklind et al. (2007a,b) criteria would select the descendants of $z \sim 6$ quasars during the passively-evolving phase near redshift $z \sim 5$. While the Wiklind et al. (2007a,b) selection was designed to find massive ($M_\star \sim 10^{11} M_\odot$) and evolved galaxies near $z \sim 5$, the agreement may be somewhat surprising given that the evolution of the simulated quasar host SED in the J-, H-, K_s-, and [3.6μm]-bands is qualitatively different than the evolving SED models used to design the Wiklind et al. (2007a,b) selection. However, we note that over the range of redshifts where the quasar host galaxy would be detectable in the GOODS and ISAAC data the simulated system resides in the locus of observed galaxies in the Wiklind et al. (2007a,b) sample in the $(J - K_s)$–$(H - [3.6\mu\mathrm{m}])$–$(K_s - [3.6\mu\mathrm{m}])$ color space. We also note that the Wiklind et al. (2007a,b) criteria are briefly satisfied by the galaxy at $z \sim 6.5$ during the height of the quasar activity, but such bright sources can be discriminated from inactive high-redshift galaxies through spectroscopic observations.

5. OBSERVABILITY

The comparisons between the redshift-dependent photometric properties of massive quasar host galaxies and color selection criteria in §4.1-4.6 demonstrate that the SEDs of the most massive high-redshift galaxies likely satisfy a variety of existing photometric selection techniques. However, these high-redshift galaxies are extremely massive and therefore extraordinarily rare. To determine whether existing or future galaxy surveys would include such rare systems in their samples, the observability of these massive galaxies must be estimated. A straightforward quantification of the observability is to calculate the fractional sky coverage and flux limit required to include and detect some defined galaxy sample. Below, we use the evolution of the quasar host galaxy SED, the ΛCDM cosmological model, and Press & Schechter (1974) theory to estimate these quantities.

The comoving volume element $\mathrm{d}V$ of a spherical redshift shell of thickness $\mathrm{d}z$ at comoving distance $r(z)$ and redshift z can be written

$$\mathrm{d}V = 4\pi r^2(z)\frac{\mathrm{d}r}{\mathrm{d}z}\mathrm{d}z \quad (18)$$

where

$$r(z) = \int_0^z \frac{\mathrm{d}r}{\mathrm{d}z'}\mathrm{d}z' = \int_0^z \frac{c\,\mathrm{d}z'}{H(z')}, \quad (19)$$

c is the speed of light, the redshift-dependent Hubble parameter for a flat universe is

$$H(z) = H_0\left[\Omega_\mathrm{M}(1+z)^3 + \Omega_\Lambda\right]^{1/2}, \quad (20)$$

and H_0 is the Hubble constant today. The number of galaxies $\mathrm{d}N$ in this comoving volume element is then simply $\mathrm{d}N = n(z)\mathrm{d}V$, where $n(z)$ is the redshift-dependent comoving number density of galaxies that comprise the sample. For the form of $n(z)$, we use the mass function proposed by Sheth & Tormen (1999) to extend the Press & Schechter (1974) theory of halo formation to model ellipsoidal collapse. Assuming an overdensity threshold $\delta_c = 1.686$ for halo collapse, we can define the quantity $\nu = \sqrt{a}\delta_c/[\sigma(M)D(z)]$ that relates the root-mean-squared fluctuations $\sigma(M)$ on a mass scale M, the linear growth factor

$$D(z) = D_0 H(z)\int_z^\infty \frac{(1+z')\mathrm{d}z'}{H^3(z')} \quad (21)$$

with D_0 normalized such that $D(z=0) = 1$, and δ_c to describe the rarity of the density peak that collapsed to form the halo of mass M. Here the constant $a = 0.707$ was determined from cosmological N-body simulations by Sheth & Tormen (1999). In terms of the peak rarity ν, the comoving number density of galaxies above some given mass M_low is then

$$n(M_\mathrm{low}, z) = \int_{\ln M_\mathrm{low}}^\infty \frac{\mathrm{d}n}{\mathrm{d}\ln m}\mathrm{d}\ln m = \Omega_m\rho_c\int_{\ln M_\mathrm{low}}^\infty \frac{A}{m\sigma}\sqrt{\frac{2}{\pi}}(1+\nu^{-2p})\nu e^{-\frac{\nu^2}{2}} \times \frac{\mathrm{d}\sigma}{\mathrm{d}\ln m}\mathrm{d}\ln m, \quad (22)$$

where the parameter $A = 0.322$ is constrained such that $\int_0^\infty (\mathrm{d}n/\mathrm{d}\ln m)\mathrm{d}\ln m = 1$ and $p = 0.3$ is determined from fitting to halo mass functions measured in cosmological simulations. If we choose M_low to correspond to the redshift-dependent virial mass of a quasar host galaxy and assume that more massive halos will host brighter galaxies, then M_low defines a luminosity-selected sample of very massive galaxies at redshift z with comoving number density $n(z)$.

To calculate an actual number N of galaxies, a redshift interval $z_\mathrm{low} \le z \le z_\mathrm{high}$ must be prescribed to define the

comoving volume that hosts the sample as

$$N(z_{\rm low}, z_{\rm high}, M_{\rm low}) = \int n(M_{\rm low}, z) {\rm d}V$$
$$= 4\pi c \int_{z_{\rm low}}^{z_{\rm high}} \frac{n(M_{\rm low}, z') r^2(z') {\rm d}z'}{H(z')}. \quad (23)$$

For a given selection criterion, such as a Lyman-break dropout, $z_{\rm low}$ will correspond to the redshift at which galaxy SEDs satisfy the color criteria. At $z_{\rm low}$ the least massive galaxy in the sample will have a magnitude $m_{\rm AB}$ that corresponds to the brightest possible magnitude limit of a survey that could detect galaxies with mass $M_{\rm low}$. Typically, for dropout criteria this magnitude limit would apply to the redder of the two bands (e.g., i_{775}-band for V_{606}-dropouts). However, such a survey would have a very small comoving volume (since $z_{\rm low} = z_{\rm high}$ in this case) and it is desirable to improve the magnitude limit to increase the comoving volume of the survey. As the magnitude limit of the survey is improved to a new $m'_{\rm AB}$, $z_{\rm high}$ increases to the epoch when galaxies with mass $M_{\rm low}$ first became brighter than $m'_{\rm AB}$. For a given photometric selection which sets $z_{\rm low}$, and survey magnitude limit $m_{\rm AB}$, the fractional sky coverage needed to detect N_d galaxies with mass greater than $M_{\rm low}$ at $z_{\rm low}$ is

$$f = N_d / N(z_{\rm low}, z_{\rm high}[m_{\rm AB}], M_{\rm low}) \quad (24)$$

While this is conceptually straightforward, there are two immediate complications. First, the correspondence between the upper redshift limit $z_{\rm high}$ and the magnitude limit $m_{\rm AB}$ depends on the redshift-dependent photometric properties of galaxies with mass $M_{\rm low}$. Second, galaxies with mass $M_{\rm low}$ at epoch $z_{\rm low}$ are evolving and will have some lower mass at higher redshifts. Fortunately, the calculations of the redshift-dependent galaxy SED described in §3 provide the desired $z_{\rm high} - m_{\rm AB}$ correspondence. For the mass accretion history the merger-tree from the Li et al. (2006) simulation is boxcar averaged with window width of ${\rm d}z = 0.3$. The resulting smooth mass accretion history increases rapidly from $z \sim 14$ to $z \sim 9$ owing to frequent mergers, and has a shape similar to the Wechsler et al. (2002) form for dark matter halo mass accretion histories. We note the observability calculation is insensitive to the exact shape of the mass accretion history as long as the rapid decline in virial mass at $z > 9$ is reproduced.

The relation between fractional sky coverage and survey limiting magnitude is plotted in Figure 11 for a variety of color selection criteria explored in 3, including V_{606}-dropout (Eq. 5, $z_{\rm low} \sim 4.5$), i_{775}-dropout (Eq. 7, $z_{\rm low} \sim 5.7$), z_{850}-dropout (Eq. 12, $z_{\rm low} \sim 6.8$), and $[3.6\mu{\rm m}] - [4.5\mu{\rm m}] > 0.3$ break ($z_{\rm low} \sim 9.1$) samples. For these color selection criteria, the quasar host galaxy virial mass in the Li et al. (2006) simulation increases from $M_{\rm low} = 5.22 \times 10^{12} h^{-1} M_\odot$ at $z_{\rm low} = 9.1$ to $M_{\rm low} = 8.01 \times 10^{12} h^{-1} M_\odot$ at $z_{\rm low} \sim 4.5$. Beginning with the brightest possible magnitude limit, corresponding to the luminosity of $M_{\rm low}$-mass galaxies at $z_{\rm low}$, the necessary fractional sky coverage declines as the sample comoving volume increases with limiting magnitude until $z_{\rm high}$ is reached. At larger (fainter) magnitudes, the fractional sky coverage becomes flat. The width of the transition region before the fractional sky coverage flattens is set by the redshift range over which the luminosity declines. For the V_{606}-, i_{775}-, and z_{850}-dropout samples, IGM absorption sets $z_{\rm high}$ to approximately the redshift when Lyα moves into the i_{775}-, z_{850}-, and J_{110}-bands, respectively. The Lyman break is dramatic at such high redshifts and, when combined with the decrease in ${\rm d}r/{\rm d}z$ and $n(z)$ with redshift, causes the fractional sky coverage to flatten quickly beyond the brightest limiting magnitude. The larger transition width for the z_{850}-dropout selection relative to the bluer color selections is set by the comparably large bandwidth of the F110W filter. For the $[3.6\mu{\rm m}] - [4.5\mu{\rm m}]$-break selection, the fractional sky coverage artificially flattens at the $[4.5\mu{\rm m}]$-band magnitude of the system at $z \sim 14$ ($[4.5\mu{\rm m}] \sim 26$), where the simulation begins. Since these galaxies are bright ($[4.5\mu{\rm m}] < 24$ to $z \sim 12$), only a relatively small fractional sky coverage is needed to detect them. However, given the decline of ${\rm d}r/{\rm d}z$ and $n(z)$ with redshift, such a sample would be dominated by systems at $z \sim 4$.

Given the rapid decline of the comoving number density n with mass $M_{\rm low}$ at fixed redshift, a useful comparison is the fractional sky coverage needed to observe systems that are less massive than the Li et al. (2006) simulated galaxy by a factor of ~ 2. Figure 11 also shows the require fractional sky coverage for these systems, assuming their photometric evolution is similar to massive galaxies and their luminosity scales with their halo mass. Such systems are clearly $\sim 10\times$ more abundant than galaxies twice their mass. These systems would have stellar masses of $7 \times 10^{11} M_\odot$, and SMBH masses $M_{\rm BH} \sim 10^9 M_\odot$, and could host quasars at $z \lesssim 6$. The virial mass of such galaxies is similar to that inferred from the clustering of quasars at in the 2dF, SDSS, and other surveys (Porciani et al. 2004; Porciani & Norberg 2006; Wake et al. 2004; Croom et al. 2005; Coil et al. 2006; Shen et al. 2007) and measurements of the quasar proximity effect (Faucher-Giguere et al. 2007; Kim & Croft 2007; Guimaraes et al. 2007), and are qualitatively similar to the system simulated by Li et al. (2006) and the large set of $z \sim 6$ merger simulations performed by Robertson et al. (2006b). The detection of the host galaxies of such quasars in Lyman-break dropout or Balmer-break samples would also provide interesting insights into the formation of massive high-redshift galaxies (for a possible sample of such systems at $z \sim 5$, see Wiklind et al. 2007a,b).

For comparison, we also show the necessary sky coverage to find objects with an abundance fixed to the comoving number density ($n \sim 4 \times 10^{-9} h^{-3} {\rm Mpc}^{-3}$) of halos with virial mass $M_{\rm vir} \gtrsim 8 \times 10^{12} h^{-1} M_\odot$ at $z \sim 6.5$ if their luminosity evolution is similar to the simulated quasar host galaxy (Fig. 11, dashed-dotted lines). Correspondingly, such systems have an abundance similar to massive quasar host galaxies when they fall in i_{775}-dropout samples. For higher-redshift selections, this estimate of the massive galaxy abundance is more favorable for finding the progenitors of $z \sim 6$ quasars and is comparable to our $M_{\rm low} = 0.5 M_{\rm vir}$ abundance estimates.

The estimated survey parameters for finding high-redshift massive galaxies can be compared with the properties of existing and future photometric surveys to gauge the likelihood for the most massive high-redshift galaxies to be found in actual observational samples. The largest existing survey is the SDSS, which has magnitude limits of $i' \sim 22.3$ and $z' \sim 20.8$ (York et al. 2000) over 8452 deg^2 [11]. While the SDSS has sufficient area to capture the most massive galaxies at redshifts as high as $z \gtrsim 12$, the bright magnitude limits and lack of infrared coverage makes the detection of extremely massive high-redshift ($z > 6$) galaxies in the SDSS implausible. Of course, as has been beautifully demonstrated, the rarer subpopulation of massive galaxies in a bright quasar phase has been detected in $\sim 1/2$ the total SDSS area (e.g., Fan et al. 2003) as the remarkable luminosity of the $z \sim 6$ quasar sample and the large sky coverage of the SDSS allows for the detection of tens of systems.

Compared with SDSS, deeper but smaller surveys have more advantageous parameters for finding Lyman-break dropouts at redshifts $z \gtrsim 4.5$. For instance, the Boötes field of the National Optical Astronomy Observatory Wide Deep Field Survey (Jannuzi & Dey 1999) has an 9.3 deg^2 field with magnitude limits of $I = 26$ and $J = 21$. While the J-band coverage is likely too shallow to detect high-redshift quasar host galaxies, this area-magnitude combination should be sufficient to find the most massive galaxies

[11] http://www.sdss.org/status/

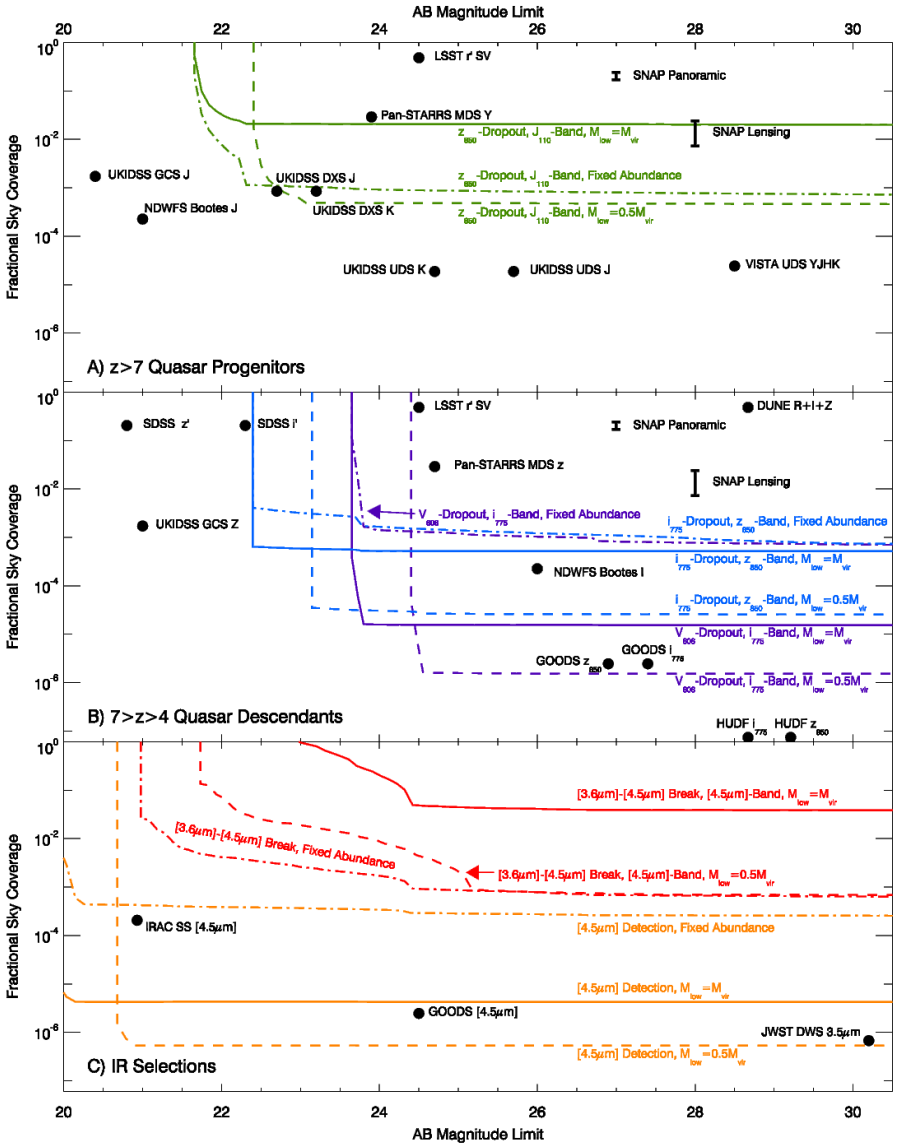

FIG. 11.— Estimated survey parameters required to find $z \gtrsim 7$ quasar progenitors (upper panel) and quasar descendants at redshifts $7 \gtrsim z \gtrsim 4$ (middle panel), or detect quasar host galaxies in the near infrared (bottom panel). Shown is the fractional sky coverage and minimum AB magnitude limit needed to build V_{606}-dropout (purple), i_{775}-dropout (blue), z_{850}-dropout (green), and $[3.6\mu\mathrm{m}] - [4.5\mu\mathrm{m}]$ break (red) samples that include a galaxy more massive than the virial mass M_{vir} (solid line) or $0.5M_{\mathrm{vir}}$ (dashed line) of the simulated $z \sim 6$ quasar host from Li et al. (2006). For comparison, the coverage needed to find objects with an abundance fixed at the number density of halos more massive than the simulated galaxy at $z \sim 6.5$ (dashed-dotted line) is also shown. As the dropout selection moves to redder bands and higher redshifts, the comoving volume and redshift interval over which massive galaxies satisfy selection criteria decreases. The comoving number density of massive galaxies, calculated using the Sheth & Tormen (1999) mass function, also declines rapidly at high-redshifts. The combination these effects requires large fractional sky coverage to find starbursting quasar progenitors at $z \gtrsim 7$ (e.g. z_{850}-dropout or $[3.6\mu\mathrm{m}] - [4.5\mu\mathrm{m}]$ break selections). The circles show the parameters of the existing Hubble UDF (i_{775}- and z_{850}-band), GOODS (i_{775}-, z_{850}-, and [4.5μm]-bands), SDSS (i'- and z'-bands), NOAO Wide Deep Field Survey (I- and J-bands), UKIRT Deep Sky Survey (Z- and J- bands for the Galactic Clusters Survey, J- and K-bands for the Deep Extra Galactic and Ultradeep Surveys), and IRAC Shallow Survey ([4.5μm]-band) observations. Future observations from the *Dark Universe Explorer* ($R+I+Z$ band) and the Ultra-deep *Visible and Infrared Telescope for Astronomy* survey (Y-, J-, H-, and K-bands) could detect $z \sim 5-6$. Even wider future surveys with redder sensitivity, such as the Pan-STARRS Medium Deep Survey (z- and Y-band), *Large Synoptic Survey Telescope* observations (r' Single Visit), and the SNAP Panoramic and Lensing surveys (error bars) could find quasar progenitors at $z \gtrsim 8$ if their two reddest-bands reach $\gtrsim 22$ AB magnitude sensitivity. A *James Webb Space Telescope* Deep-Wide Survey (Gardner et al. 2006) would need to be considerably wider to find the $z > 7$ starbursting progenitors of $z \sim 6$ quasars. Also shown is the fractional sky coverage to detect $z \sim 6$ quasar host galaxies at $z \gtrsim 4$ in the [4.5μm]-band (orange lines), which only requires a small-area survey with a $[4.5\mu\mathrm{m}] \sim 20.5$ magnitude limit.

at $z \sim 4.5-5$ in V-dropout samples. The accompanying IRAC Shallow Survey (Eisenhardt et al. 2004), with 8.5 deg^2 coverage down to $[4.5\mu\mathrm{m}] \approx 20.9$ would detect these systems as well as higher-redshift I-dropouts in the NOAO NWDFS (for galaxies with photometric redshifts $z \lesssim 2$, see Brodwin et al. 2006). The *United Kingdom Infrared Telescope* Deep Sky Survey (UKIDSS, Warren & Hewett 2002; Warren et al. 2007) includes a Galaxy Cluster Survey (GCS, 70.9 deg^2 area to $Z \approx 21$ and $J \approx 20.4$), a Deep Extragalactic Survey (DXS, 35 deg^2 area to $J \approx 23.2$ and $K = 22.7$), and an Ultradeep Survey (UDS, 0.77 deg^2 area to $J \approx 25.7$ and $K \approx 24.7$, see Lawrence et al. 2006). While the UKIDSS GCS is too shallow to find the very massive galaxies we model, the UKIDSS DXS and UDS could detect such systems in the J- and K-bands at $z \gtrsim 4$. The UKIDSS DXS may even have enough area to detect massive quasar progenitors at $z \gtrsim 7$ (see also Warren & Hewett 2002), which would be an exciting prospect, but the lack of deep coverage at shorter wavelengths in the DXS may limit its ability to identify such systems as Lyman-break dropouts. A proposed UDS with the Visible and Infrared Survey Telescope for Astronomy (VISTA) could reach 5-σ AB limiting magnitudes of $Y = 26.7$, $J = 26.6$,

$H = 26.1$, and $K_s = 25.6$ over a $\sim 1\,\mathrm{deg}^2$ field (M. Franx, private communication). While the proposed VISTA observations would be significantly deeper than the UKDISS UDS or the NDWFS, the size of the field could limit the survey to finding $z \sim 6$ quasar host galaxies at $z \lesssim 5$.

The GOODS observations that cover 365 arcmin^2 reach depths of $i_{775} \approx 27.4$ and $z_{850} \approx 26.9$ with ACS (Giavalisco et al. 2004b) and $[4.5\mu\mathrm{m}] = 24.5$ with IRAC (Dickinson et al. 2003). The GOODS V_{606}-dropout sample has the necessary sky coverage to include a $M_\star \sim 5 \times 10^{11} M_\odot$ stellar mass galaxy at $z \sim 4-5$ with $i_{775} \sim 25$ and detections in all redder bands, though we are not aware of any such systems in the current GOODS data. Less massive ($M_\star \sim 10^{11} M_\odot$) systems are much more abundant and our estimate would predict a handful of such $z \sim 5$ systems in GOODS, which may have already been detected (e.g., Stark et al. 2006). The HUDF data, with an 11 arcmin^2 area and magnitude limits of $i_{775} = 29.21$ and $z_{850} = 28.67$ (Beckwith et al. 2006), is simply too narrow to include objects as rare as $z \sim 6$ quasar host galaxies. We note briefly that these simulations suggest that to detect $M_\star \sim 5 \times 10^{11} M_\odot$ galaxies in J_{110}-dropout samples at $z \gtrsim 7$ (e.g. Mobasher et al. 2005, see also Chen & Marzke (2004) and Dunlop et al. (2006)), a survey 3-4 orders of magnitude larger than the HUDF would be necessary.

Future surveys with wide area coverage and deep imaging have a substantially better opportunity to detect the starbursting progenitors of $z \sim 6$ quasars. The Pan-STARRS project is planning a $1200\,\mathrm{deg}^2$ Medium Deep Survey with magnitude limits of $z_{0.89\mu\mathrm{m}} = 24.7$ and $Y_{1.02\mu\mathrm{m}} = 23.9$[12], which could find massive quasar progenitors in z-band dropout samples at $z \gtrsim 7$. The *Large Synoptic Survey Telescope* would make short work of finding the most massive high-redshift galaxies if its Y-band Single Visit Depth is comparable to its target $r = 24.5$ depth[13]. The *Supernovae Acceleration Probe* (SNAP) is planning a weak lensing survey of $300 - 1000\,\mathrm{deg}^2$ to $m_{\mathrm{AB}} = 28$ and a wide-area ($7000 - 10000\,\mathrm{deg}^2$) survey with a depth of $m_{\mathrm{AB}} = 27$ [14]. If a near-IR HgCdTe device flies with the mission and reaches similar sensitivities down to $\lambda \sim 1.5\mu$m over the same area, SNAP could detect the progenitors of $z \sim 6$ quasars at redshifts approaching $z \sim 10$. The *Dark Universe Explorer* mission will survey $20,000\,\mathrm{deg}^2$ with a composite $R+I+Z$-band in the red optical and will reach an effective $I \sim 24.5$ limiting magnitude (Réfrégier et al. 2006), which should detect massive spheroids at $z \sim 5$. The *James Webb Space Telescope* easily has enough sensitivity to detect massive quasar progenitors out to $z \gtrsim 15$ (with stellar masses $M_\star \lesssim 10^{10} M_\odot$), but currently suggested observations, such as a Deep-Wide Survey with a 100 arcmin^2 area and limiting magnitude of $m_{\mathrm{AB}} \approx 30.2$ at $\lambda = 3.5\mu$m (Gardner et al. 2006), would be too narrow to find such rare objects at the highest redshifts.

6. DISCUSSION

The discovery of very massive high-redshift galaxies would provide an interesting new perspective on the structure formation process. While the larger abundance of less-massive galaxies allow the redshift evolution of such systems to be researched by characterizing the statistical properties of populations of objects, the rarity of the most massive galaxies will likely limit our ability to draw inferences about their formation from population studies. If the most massive galaxies at the current epoch were a largely heterogeneous population, their rarity could prove a significant limitation in unravelling the various modes for their formation.

[12] http://pan-starrs.ifa.hawaii.edu/
[13] http://www.lsst.org/Science/docs/SRD_summary.pdf
[14] http://snap.lbl.gov

Fortunately, the most massive galaxies today are a roughly homogeneous population. Studies of the color bimodality of galaxies (e.g., Strateva et al. 2001; Bell et al. 2004; Baldry et al. 2004) show that the most luminous galaxies are almost uniformly red ($g' - r' \gtrsim 1.2$). Such galaxies populate the center of galaxy clusters and their properties are roughly uniform between clusters at the same epoch (e.g., Bower et al. 1992; Gladders & Yee 2000). Importantly, these massive galaxies have been demonstrated to contain supermassive black holes with mass $M_{\mathrm{BH}} \gtrsim 10^9 M_\odot$ (i.e. M87, Harms et al. 1994; Macchetto et al. 1997). The large SMBH masses directly connect the population of the most massive galaxies at low redshift to the luminous quasars at $z \sim 6$, since $10^9 M_\odot$ SMBHs are the most credible engine to power $z \sim 6$ quasars, and suggest that the most luminous high-redshift quasars evolve into a roughly homogeneous population at the current epoch. Our calculations support this possibility, under the condition that the most massive galaxies undergo little star formation and their stellar populations evolve passively from $z \sim 4$ to the present. Observed cluster ellipticals have stellar formation epochs of at least $z \gtrsim 2$ (e.g., van Dokkum & Franx 2001; Gebhardt et al. 2003). We note that this picture does not preclude future major mergers between spheroids at lower redshifts (e.g., van Dokkum 2005; Bell et al. 2006), which may have some relation to core-cusp bimodality (e.g., Faber et al. 1997; Lauer et al. 2006, Kormendy et al., in preparation, Krause et al., in preparation, though see Ferrarese et al. (2006)) that is the primary heterogeneity in massive galaxies. Even so, this bimodality exists primarily in systems with $M_V > -22$, with more luminous systems mostly displaying surface brightness cores.

The connection between the most massive galaxies in the present epoch and quasars at $z \sim 6$, forged by their shared SMBH masses, and the uniformity of the most massive local galaxies permits an argument for a single evolutionary scenario for the formation of the most massive galaxies from very high-redshifts to the present day. The appeal of a single mode of formation for the most massive galaxies stems primarily from the difficulty in forming luminous quasars at high-redshifts with $\gtrsim 10^9 M_\odot$ SMBHs, the problem popularized by Efstathiou & Rees (1988). Finding a robust way of growing SMBHs quickly in the limited time available before $z \sim 6$ is problematic, but the success of the Li et al. (2006) simulation of $z \sim 6$ quasar in producing a SMBH with a mass of $M_{\mathrm{BH}} > 10^9 M_\odot$ has provided some hope that high-redshift quasars can be explained naturally in the context of the formation of rare density peaks in our ΛCDM cosmology. The calculations performed in this paper provide a detailed characterization of the observable ramifications of this scenario, the foremost being the possible detection of the star-bursting progenitors of $z \sim 6$ quasars at higher redshifts ($z \gtrsim 6$) with massive stellar populations ($M_\star \sim 10^{11.5-12.0}$) in wide-area, Lyman-break dropout samples or through wide-area IR searches for systems with rest-frame optical breaks at $z \sim 9$ and stellar masses of $M_\star \sim 10^{11} M_\odot$.

7. CONCLUSIONS

Combining hydrodynamical simulations of the hierarchical formation of a $z \sim 6$ quasar (Li et al. 2006), stellar population synthesis models (Leitherer et al. 1999; Vázquez & Leitherer 2005), AGN spectral templates (Vanden Berk et al. 2001; Marconi et al. 2004), models for the wavelength-dependent attenuation owing to interstellar and intergalactic absorption (Calzetti et al. 1994, 2000; Madau 1995), and the transmissivity of telescopes, filters, and detectors, the photometric properties of a massive $z \sim 6$ quasar host galaxy are calculated at redshifts $z \sim 4 - 14$. The photometric properties of the quasar host galaxy reflect three main evolutionary phases in its formation; a starburst-dominated phase at $z \gtrsim 6.7$, an AGN phase at $5.7 \lesssim z \lesssim 6.7$ that includes optical quasar

activity at $z \sim 6.5$, and a passive-evolution phase at $z \lesssim 5.7$. The photometric properties of the system are then compared with color-selection techniques for finding high-redshift galaxies. The main findings of these calculations follow.

- At very high-redshifts $z \sim 6.7 - 14$, multiple gas-rich mergers gives rise to star formation rates of SFR $\sim 10^3 - 10^4$, building a stellar spheroid of $> 10^{12} M_\odot$ by $z \sim 7$ (Li et al. 2006). Our calculations show that these star formation rates naturally give rise to a photometric starburst phase with strong rest-frame UV and blue optical emission that satisfy HST ACS/NICMOS Lyman-break criteria for galaxies at $z > 7$ (e.g. Bouwens et al. 2004; Bouwens & Illingworth 2006). Over this epoch, the near-infrared luminosity of the system peaks at $z \sim 8.5$ with $J_{110} \sim 21.7$, $H_{160} \sim 20.5$, and $K_s \sim 20.5$ in AB magnitudes.
- During the phase of AGN activity ($5.7 \lesssim z \lesssim 6.7$), IGM absorption blue-ward of Lyα causes the system to satisfy both F775W-band dropout criteria for LBGs in GOODS (e.g. Stanway et al. 2003; Giavalisco et al. 2004a) and the SDSS i'-band dropout selection for high-redshift quasars (e.g. Fan et al. 2003). At higher redshifts IGM absorption begins to attenuate the z'-band flux and push the quasar host galaxy towards the locus of L-dwarfs in the $z' - J_{\rm Vega}$ vs. $i' - z'$ color-color space. During this phase, the quasar host galaxy is usually ~ 2 z'-band magnitudes fainter than the Fan et al. (2003) sample selection flux limit.
- At lower redshifts ($z \lesssim 5.7$) after the starburst and AGN activity has declined, the quasar host galaxy satisfies V_{606}-dropout criteria for galaxies at $z \sim 5$ (e.g., Giavalisco et al. 2004b; Yan et al. 2005). The quasar descendant also satisfies Balmer break selection techniques designed to identify massive and evolved galaxies at $z \sim 5$ (e.g., Wiklind et al. 2007a,b).
- Throughout the photometric evolution of the quasar host galaxy, the system satisfies *Spitzer* IRAC color-color selections for AGN (Stern et al. 2005b) and high-redshift galaxies (Barmby et al. 2004).
- The area and depth necessary to find the most massive high-redshift galaxies in photometric surveys is estimated from our photometric modeling and the redshift-dependent abundance of dark matter halos (Press & Schechter 1974; Sheth & Tormen 1999). Existing surveys, such as the IRAC Shallow Survey or NOAO Deep-Wide Field Survey, may be large enough to find the massive $z \sim 4$ descendants of $z \sim 6$ quasars. Surveys of significant fractions of the sky ($\gtrsim 0.001$) in the z_{850} and J_{110} or similar bands, such as the UKIRT Deep Sky Survey, will be necessary to find the star-bursting progenitors of $z \sim 6$ at high-redshifts ($z > 7$). Future surveys, such as Pan-STARRS, the *Large Synoptic Survey Telescope*, or the *Supernovae Acceleration Probe*, should have the necessary area and depth to find the most massive high-redshift galaxies.
- If future surveys contain a J_{110}-dropout massive quasar progenitor at $z \sim 10$, evidence for star formation at $z \gtrsim 12$ in the form of a Balmer/4000Å break could be detected in the $[3.6\mu{\rm m}] - [4.5\mu{\rm m}]$ vs. $[4.5\mu{\rm m}] - [5.8\mu{\rm m}]$ color-color space.

The remarkable luminosity and early-formation time of the massive progenitor galaxies of $z \sim 6$ quasars could enable their detection at very high-redshifts $z \gtrsim 7$. The detection of these massive galaxies would help settle outstanding questions about how the rarest structures form in the ΛCDM cosmology and what evolutionary processes give rise to $z \sim 6$ quasars. As observations must ultimately determine the existence and properties of the most massive high-redshift galaxies, we eagerly anticipate future efforts to detect and characterize these extraordinary quasar progenitors.

BER gratefully acknowledges support from a Spitzer Fellowship, through a NASA grant administered by the Spitzer Science Center, and thanks Hsiao-Wen Chen, Tiziana Di Matteo, Volker Springel, Marijn Franx, and Andrew Zentner for helpful comments. BER also thanks Dr. Wiklind for early access to his results before publication. This work was supported in part by NSF grants ACI 96-19019, AST 00-71019, AST 02-06299, and AST 03-07690, and NASA ATP grants NAG5-12140, NAG5-13292, and NAG5-13381. The simulations were performed at the Center for Parallel Astrophysical Computing at Harvard-Smithsonian Center for Astrophysics.

REFERENCES

Abel, T., Bryan, G. L., & Norman, M. L. 2002, Science, 295, 93
Baldry, I. K., Glazebrook, K., Brinkmann, J., Ivezić, Ž., Lupton, R. H., Nichol, R. C., & Szalay, A. S. 2004, ApJ, 600, 681
Barmby, P., et al. 2004, ApJS, 154, 97
Barnes, J. E., & Hernquist, L. 1996, ApJ, 471, 115
Barnes, J. E., & Hernquist, L. E. 1991, ApJ, 370, L65
Barth, A. J., Ho, L. C., & Sargent, W. L. W. 2003, ApJ, 583, 134
Barton, E. J., Davé, R., Smith, J.-D. T., Papovich, C., Hernquist, L., & Springel, V. 2004, ApJ, 604, L1
Baugh, C. M., Cole, S., Frenk, C. S., & Lacey, C. G. 1998, ApJ, 498, 504
Beckwith, S. V. W., et al. 2006, AJ, 132, 1729
Bell, E. F., et al. 2006, ApJ, 640, 241
—. 2004, ApJ, 608, 752
Bershady, M. A., Charlton, J. C., & Geoffroy, J. M. 1999, ApJ, 518, 103
Bertoldi, F., Carilli, C. L., Cox, P., Fan, X., Strauss, M. A., Beelen, A., Omont, A., & Zylka, R. 2003, A&A, 406, L55
Bohlin, R. C., Savage, B. D., & Drake, J. F. 1978, ApJ, 224, 132
Bondi, H. 1952, MNRAS, 112, 195
Bouwens, R. J., & Illingworth, G. D. 2006, Nature, 443, 189
Bouwens, R. J., et al. 2003, ApJ, 595, 589
—. 2004, ApJ, 616, L79
Bower, R. G., Lucey, J. R., & Ellis, R. S. 1992, MNRAS, 254, 601
Bremer, M. N., Jensen, J. B., Lehnert, M. D., Schreiber, N. M. F., & Douglas, L. 2004, ApJ, 615, L1
Brodwin, M., et al. 2006, ApJ, 651, 791
Bromm, V., & Larson, R. B. 2004, ARA&A, 42, 79
Bullock, J. S., Kolatt, T. S., Sigad, Y., Somerville, R. S., Kravtsov, A. V., Klypin, A. A., Primack, J. R., & Dekel, A. 2001, MNRAS, 321, 559
Bunker, A. J., Stanway, E. R., Ellis, R. S., & McMahon, R. G. 2004, MNRAS, 355, 374
Bunker, A. J., Stanway, E. R., Ellis, R. S., McMahon, R. G., & McCarthy, P. J. 2003, MNRAS, 342, L47
Calzetti, D. 1997, AJ, 113, 162
Calzetti, D., Armus, L., Bohlin, R. C., Kinney, A. L., Koornneef, J., & Storchi-Bergmann, T. 2000, ApJ, 533, 682
Calzetti, D., Kinney, A. L., & Storchi-Bergmann, T. 1994, ApJ, 429, 582
Cardelli, J. A., Clayton, G. C., & Mathis, J. S. 1989, ApJ, 345, 245
Carilli, C. L., et al. 2004, AJ, 128, 997
Chary, R.-R., Stern, D., & Eisenhardt, P. 2005, ApJ, 635, L5
Chen, H.-W., & Marzke, R. O. 2004, ApJ, 615, 603
Cohen, M., Wheaton, W. A., & Megeath, S. T. 2003, AJ, 126, 1090
Coil, A. L., Newman, J. A., Cooper, M. C., Davis, M., Faber, S. M., Koo, D. C., & Willmer, C. N. A. 2006, ApJ, 644, 671
Cowie, L. L., & Hu, E. M. 1998, AJ, 115, 1319
Cox, A. N. 2000, Allen's astrophysical quantities (Allen's astrophysical quantities, 4th ed. Publisher: New York: AIP Press; Springer, 2000. Editedy by Arthur N. Cox. ISBN: 0387987460)
Cox, T. J., Di Matteo, T., Hernquist, L., Hopkins, P. F., Robertson, B., & Springel, V. 2006a, ApJ, 643, 692

Cox, T. J., Dutta, S. N., Di Matteo, T., Hernquist, L., Hopkins, P. F., Robertson, B., & Springel, V. 2006b, ApJ, 650, 791
Croom, S. M., et al. 2005, MNRAS, 356, 415
Daddi, E., et al. 2003, ApJ, 588, 50
Davé, R., Finlator, K., & Oppenheimer, B. D. 2006, MNRAS, 370, 273
Davé, R., Hernquist, L., Katz, N., & Weinberg, D. H. 1999, ApJ, 511, 521
Di Matteo, T., Springel, V., & Hernquist, L. 2005, Nature, 433, 604
Dickinson, M., Giavalisco, M., & The Goods Team. 2003, in The Mass of Galaxies at Low and High Redshift, ed. R. Bender & A. Renzini, 324–+
Dickinson, M., et al. 2004, ApJ, 600, L99
Dunlop, J. S., Cirasuolo, M., & McLure, R. J. 2006, ArXiv Astrophysics e-prints
Efstathiou, G., & Rees, M. J. 1988, MNRAS, 230, 5P
Egami, E., et al. 2005, ApJ, 618, L5
Eisenhardt, P. R., et al. 2004, ApJS, 154, 48
Ellis, R., Santos, M. R., Kneib, J.-P., & Kuijken, K. 2001, ApJ, 560, L119
Eyles, L., Bunker, A., Ellis, R., Lacy, M., Stanway, E., Stark, D., & Chiu, K. 2006, ArXiv Astrophysics e-prints
Eyles, L. P., Bunker, A. J., Stanway, E. R., Lacy, M., Ellis, R. S., & Doherty, M. 2005, MNRAS, 364, 443
Faber, S. M., et al. 1997, AJ, 114, 1771
Fabian, A. C. 1999, MNRAS, 308, L39
Fagotto, F., Bressan, A., Bertelli, G., & Chiosi, C. 1994, A&AS, 105, 29
Fan, X., et al. 2004, AJ, 128, 515
—. 2001a, AJ, 122, 2833
—. 2006, AJ, 131, 1203
—. 2001b, AJ, 121, 31
—. 2003, AJ, 125, 1649
—. 2000, AJ, 120, 1167
Faucher-Giguere, C.-A., Lidz, A., Zaldarraiga, M., & Hernquist, L. 2007, ArXiv Astrophysics e-prints
Fazio, G. G., et al. 2004, ApJS, 154, 10
Ferrarese, L., et al. 2006, ApJS, 164, 334
Ferrarese, L., & Merritt, D. 2000, ApJ, 539, L9
Finlator, K., Davé, R., Papovich, C., & Hernquist, L. 2006, ApJ, 639, 672
Fitzpatrick, E. L. 1986, AJ, 92, 1068
Ford, H. C., et al. 1998, in Proc. SPIE Vol. 3356, p. 234-248, Space Telescopes and Instruments V, ed. P. Y. Bely & J. B. Breckinridge
Franx, M., et al. 2003, ApJ, 587, L79
Fukugita, M., Ichikawa, T., Gunn, J. E., Doi, M., Shimasaku, K., & Schneider, D. P. 1996, AJ, 111, 1748
Gao, L., White, S. D. M., Jenkins, A., Frenk, C. S., & Springel, V. 2005, MNRAS, 363, 379
Gardner, J. P., et al. 2006, Space Science Reviews, 123, 485
Gebhardt, K., et al. 2000, ApJ, 539, L13
—. 2003, ApJ, 597, 239
Genzel, R., et al. 1998, ApJ, 498, 579
Giavalisco, M., et al. 2004a, ApJ, 600, L103
—. 2004b, ApJ, 600, L93
Gladders, M. D., & Yee, H. K. C. 2000, AJ, 120, 2148
Gordon, K. D., Clayton, G. C., Misselt, K. A., Landolt, A. U., & Wolff, M. J. 2003, ApJ, 594, 279
Granato, G. L., De Zotti, G., Silva, L., Bressan, A., & Danese, L. 2004, ApJ, 600, 580
Grazian, A., et al. 2006, A&A, 449, 951
Guimaraes, R. N., Petitjean, P., Rolline, E. B., De Carvalho, R. R., Djorgovski, G., Srianand, R., Aghaee, A., & Castro, S. 2007, ArXiv Astrophysics e-prints
Harford, A. G., & Gnedin, N. Y. 2003, ApJ, 597, 74
Häring, N., & Rix, H.-W. 2004, ApJ, 604, L89
Harms, R. J., et al. 1994, ApJ, 435, L35
Hernquist, L. 1989, Nature, 340, 687
Hopkins, P. F., Hernquist, L., Cox, T. J., Di Matteo, T., Robertson, B., & Springel, V. 2006a, ApJS, 163, 1
Hopkins, P. F., Hernquist, L., Cox, T. J., Robertson, B., & Krause, E. 2007a, ArXiv Astrophysics e-prints
Hopkins, P. F., Hernquist, L., Cox, T. J., Robertson, B., & Springel, V. 2006b, ApJS, 163, 50
Hopkins, P. F., Hernquist, L., Martini, P., Cox, T. J., Robertson, B., Di Matteo, T., & Springel, V. 2005, ApJ, 625, L71
Hopkins, P. F., Lidz, A., Hernquist, L., Coil, A. L., Myers, A. D., Cox, T. J., & Spergel, D. N. 2006c, ArXiv Astrophysics e-prints
Hopkins, P. F., Richards, G. T., & Hernquist, L. 2007b, ApJ, 654, 731
Hu, E. M., & Cowie, L. L. 2006, Nature, 440, 1145
Hu, E. M., Cowie, L. L., McMahon, R. G., Capak, P., Iwamuro, F., Kneib, J.-P., Maihara, T., & Motohara, K. 2002, ApJ, 568, L75
Irwin, M., McMahon, R. G., & Hazard, C. 1991, in ASP Conf. Ser. 21: The Space Distribution of Quasars, ed. D. Crampton, 117–126
Iye, M., et al. 2006, Nature, 443, 186
Jannuzi, B. T., & Dey, A. 1999, in ASP Conf. Ser. 191: Photometric Redshifts and the Detection of High Redshift Galaxies, ed. R. Weymann, L. Storrie-Lombardi, M. Sawicki, & R. Brunner, 111–+
Kashikawa, N., et al. 2006, ApJ, 648, 7
Katz, N., Hernquist, L., & Weinberg, D. H. 1992, ApJ, 399, L109
Kauffmann, G., Colberg, J. M., Diaferio, A., & White, S. D. M. 1999, MNRAS, 303, 188
Kauffmann, G., & Haehnelt, M. 2000, MNRAS, 311, 576
Kennicutt, R. C. 1998, ApJ, 498, 541
Kim, Y.-R., & Croft, R. 2007, ArXiv Astrophysics e-prints
King, A. 2003, ApJ, 596, L27
Kodaira, K., et al. 2003, PASJ, 55, L17
Koester, B. P., et al. 2007, ArXiv Astrophysics e-prints
Kormendy, J., & Richstone, D. 1995, ARA&A, 33, 581
Kroupa, P. 2001, MNRAS, 322, 231
—. 2002, Science, 295, 82
Kurk, J. D., Cimatti, A., di Serego Alighieri, S., Vernet, J., Daddi, E., Ferrara, A., & Ciardi, B. 2004, A&A, 422, L13
Labbé, I., Bouwens, R., Illingworth, G. D., & Franx, M. 2006, ApJ, 649, L67
Labbé, I., et al. 2005, ApJ, 624, L81
Lanzetta, K. M., Yahil, A., & Fernandez-Soto, A. 1996, Nature, 381, 759
Larson, R. B., & Tinsley, B. M. 1978, ApJ, 219, 46
Lauer, T. R., et al. 2006, ArXiv Astrophysics e-prints
Lawrence, A., et al. 2006, ArXiv Astrophysics e-prints
Lee, K.-S., Giavalisco, M., Gnedin, O. Y., Somerville, R. S., Ferguson, H. C., Dickinson, M., & Ouchi, M. 2006, ApJ, 642, 63
Lehnert, M. D., & Bremer, M. 2003, ApJ, 593, 630
Leitherer, C., et al. 1999, ApJS, 123, 3
Li, Y., et al. 2006, ArXiv Astrophysics e-prints
Lynden-Bell, D. 1969, Nature, 223, 690
Macchetto, F., Marconi, A., Axon, D. J., Capetti, A., Sparks, W., & Crane, P. 1997, ApJ, 489, 579
Madau, P. 1995, ApJ, 441, 18
Madau, P., Ferguson, H. C., Dickinson, M. E., Giavalisco, M., Steidel, C. C., & Fruchter, A. 1996, MNRAS, 283, 1388
Magdziarz, P., & Zdziarski, A. A. 1995, MNRAS, 273, 837
Magorrian, J., et al. 1998, AJ, 115, 2285
Maiolino, R., Schneider, R., Oliva, E., Bianchi, S., Ferrara, A., Mannucci, F., Pedani, M., & Roca Sogorb, M. 2004, Nature, 431, 533
Marconi, A., et al. 2003, ApJ, 586, 868
Marconi, A., Risaliti, G., Gilli, R., Hunt, L. K., Maiolino, R., & Salvati, M. 2004, MNRAS, 351, 169
McKee, C. F., & Ostriker, J. P. 1977, ApJ, 218, 148
Mihos, J. C., & Hernquist, L. 1994, ApJ, 431, L9
—. 1996, ApJ, 464, 641
Mo, H. J., Mao, S., & White, S. D. M. 1998, MNRAS, 295, 319
Mobasher, B., et al. 2005, ApJ, 635, 832
Nagamine, K., Cen, R., Furlanetto, S. R., Hernquist, L., Night, C., Ostriker, J. P., & Ouchi, M. 2006, New Astronomy Review, 50, 29
Nagamine, K., Cen, R., Hernquist, L., Ostriker, J. P., & Springel, V. 2005a, ApJ, 627, 608
—. 2005b, ApJ, 618, 23
Nagamine, K., Springel, V., & Hernquist, L. 2004, MNRAS, 348, 421
Narayanan, D., et al. 2006, ApJ, Submitted
Night, C., Nagamine, K., Springel, V., & Hernquist, L. 2006, MNRAS, 366, 705
Noguchi, M. 1988, A&A, 203, 259
Oke, J. B. 1974, ApJS, 27, 21
Ouchi, M., et al. 2005, ApJ, 620, L1

—. 2004, ApJ, 611, 660
Overzier, R. A., Bouwens, R. J., Illingworth, G. D., & Franx, M. 2006, ArXiv Astrophysics e-prints
Papovich, C., Dickinson, M., & Ferguson, H. C. 2001, ApJ, 559, 620
Papovich, C., et al. 2006, ApJ, 640, 92
Pei, Y. C. 1992, ApJ, 395, 130
Porciani, C., Magliocchetti, M., & Norberg, P. 2004, MNRAS, 355, 1010
Porciani, C., & Norberg, P. 2006, MNRAS, 371, 1824
Power, C., Navarro, J. F., Jenkins, A., Frenk, C. S., White, S. D. M., Springel, V., Stadel, J., & Quinn, T. 2003, MNRAS, 338, 14
Press, W. H., & Schechter, P. 1974, ApJ, 187, 425
Reddy, N. A., & Steidel, C. C. 2004, ApJ, 603, L13
Reddy, N. A., Steidel, C. C., Erb, D. K., Shapley, A. E., & Pettini, M. 2006, ArXiv Astrophysics e-prints
Réfrégier, A., et al. 2006, in Proc. SPIE Vol. 6265, p. 62651Y, Space Telescopes and Instrumentation I, ed. J. C. Mather, H. A. MacEwen & M. W. M. de Graauw
Richard, J., Pello, R., Schaerer, D., Le Borgne, J.-F., & Kneib, J.-P. 2006, ArXiv Astrophysics e-prints
Robertson, B., Cox, T. J., Hernquist, L., Franx, M., Hopkins, P. F., Martini, P., & Springel, V. 2006a, ApJ, 641, 21
Robertson, B., Hernquist, L., Cox, T. J., Di Matteo, T., Hopkins, P. F., Martini, P., & Springel, V. 2006b, ApJ, 641, 90
Rodrigues, C. V., Magalhaes, A. M., Coyne, G. V., & Piirola, V. 1997, ApJ, 485, 618
Salpeter, E. E. 1955, ApJ, 121, 161
Sanders, D. B., & Mirabel, I. F. 1996, ARA&A, 34, 749
Sanders, D. B., Soifer, B. T., Elias, J. H., Madore, B. F., Matthews, K., Neugebauer, G., & Scoville, N. Z. 1988a, ApJ, 325, 74
Sanders, D. B., Soifer, B. T., Elias, J. H., Neugebauer, G., & Matthews, K. 1988b, ApJ, 328, L35
Santos, M. R. 2004, MNRAS, 349, 1137
Schmidt, M. 1959, ApJ, 129, 243
Schneider, D. P., et al. 2001, AJ, 121, 1232
Schneider, D. P., Schmidt, M., & Gunn, J. E. 1991, AJ, 101, 2004
Shapley, A. E., Steidel, C. C., Erb, D. K., Reddy, N. A., Adelberger, K. L., Pettini, M., Barmby, P., & Huang, J. 2005, ApJ, 626, 698
Shen, Y., et al. 2007, ArXiv Astrophysics e-prints
Sheth, R. K., & Tormen, G. 1999, MNRAS, 308, 119
Silk, J., & Rees, M. J. 1998, A&A, 331, L1
Skrutskie, M. F., et al. 1997, in ASSL Vol. 210: The Impact of Large Scale Near-IR Sky Surveys, ed. F. Garzon, N. Epchtein, A. Omont, B. Burton, & P. Persi, 25–+
Soifer, B. T., et al. 1984, ApJ, 278, L71
Soifer, B. T., Sanders, D. B., Madore, B. F., Neugebauer, G., Danielson, G. E., Elias, J. H., Lonsdale, C. J., & Rice, W. L. 1987, ApJ, 320, 238
Somerville, R. S., Primack, J. R., & Faber, S. M. 2001, MNRAS, 320, 504
Spergel, D. N., et al. 2003, ApJS, 148, 175
Spinrad, H., Stern, D., Bunker, A., Dey, A., Lanzetta, K., Yahil, A., Pascarelle, S., & Fernández-Soto, A. 1998, AJ, 116, 2617
Springel, V. 2005, MNRAS, 364, 1105
Springel, V., Di Matteo, T., & Hernquist, L. 2005a, ApJ, 620, L79
—. 2005b, MNRAS, 361, 776
Springel, V., & Hernquist, L. 2003, MNRAS, 339, 289
Stanway, E. R., Bunker, A. J., & McMahon, R. G. 2003, MNRAS, 342, 439
Stanway, E. R., Bunker, A. J., McMahon, R. G., Ellis, R. S., Treu, T., & McCarthy, P. J. 2004a, ApJ, 607, 704
Stanway, E. R., et al. 2004b, ApJ, 604, L13
Stanway, E. R., McMahon, R. G., & Bunker, A. J. 2005, MNRAS, 359, 1184
Stark, D. P., Bunker, A. J., Ellis, R. S., Eyles, L. P., & Lacy, M. 2006, ArXiv Astrophysics e-prints
Steidel, C. C., Pettini, M., & Hamilton, D. 1995, AJ, 110, 2519
Steidel, C. C., Giavalisco, M., Pettini, M., Dickinson, M., & Adelberger, K. L. 1996, ApJ, 462, L17+
Steidel, C. C., & Hamilton, D. 1992, AJ, 104, 941
—. 1993, AJ, 105, 2017
Stern, D., et al. 2005a, ApJ, 631, 163
Stern, D., Yost, S. A., Eckart, M. E., Harrison, F. A., Helfand, D. J., Djorgovski, S. G., Malhotra, S., & Rhoads, J. E. 2005b, ApJ, 619, 12
Stiavelli, M., Fall, S. M., & Panagia, N. 2004, ApJ, 610, L1
Strateva, I., et al. 2001, AJ, 122, 1861
Taniguchi, Y., et al. 2005, PASJ, 57, 165
Telfer, R. C., Zheng, W., Kriss, G. A., & Davidsen, A. F. 2002, ApJ, 565, 773
Thompson, R. I., et al. 2005, AJ, 130, 1
Toomre, A. 1977, in Evolution of Galaxies and Stellar Populations, 401–+
Toomre, A., & Toomre, J. 1972, ApJ, 178, 623
Tremaine, S., et al. 2002, ApJ, 574, 740
van Dokkum, P. G. 2005, AJ, 130, 2647
van Dokkum, P. G., & Franx, M. 2001, ApJ, 553, 90
van Dokkum, P. G., et al. 2004, ApJ, 611, 703
Vanden Berk, D. E., et al. 2001, AJ, 122, 549
Vanzella, E., et al. 2006, A&A, 454, 423
Vázquez, G. A., & Leitherer, C. 2005, ApJ, 621, 695
Verma, A., Lehnert, M. D., Foerster Schreiber, N. M., Bremer, M. N., & Douglas, L. 2007, ArXiv Astrophysics e-prints
Vignali, C., Brandt, W. N., & Schneider, D. P. 2003, AJ, 125, 433
Volonteri, M., Haardt, F., & Madau, P. 2003, ApJ, 582, 559
Wake, D. A., et al. 2004, ApJ, 610, L85
Walter, F., et al. 2003, Nature, 424, 406
Walter, F., Carilli, C., Bertoldi, F., Menten, K., Cox, P., Lo, K. Y., Fan, X., & Strauss, M. A. 2004, ApJ, 615, L17
Warren, S., & Hewett, P. 2002, in ASP Conf. Ser. 283: A New Era in Cosmology, ed. N. Metcalfe & T. Shanks, 369–+
Warren, S. J., et al. 2007, MNRAS, 375, 213
Warren, S. J., Hewett, P. C., Irwin, M. J., McMahon, R. G., & Bridgeland, M. T. 1987, Nature, 325, 131
Wechsler, R. H., Bullock, J. S., Primack, J. R., Kravtsov, A. V., & Dekel, A. 2002, ApJ, 568, 52
Weinberg, D. H., Hernquist, L., & Katz, N. 2002, ApJ, 571, 15
Werner, M. W., et al. 2004, ApJS, 154, 1
Wiklind, T., Mobasher, B., Dickinson, M., Ferguson, H. C., Giavalisco, M., Grogin, N. A., & Panagia, N. 2007a, IAU Symposium, 235, 368
Wiklind, T., Dickinson, M., Ferguson, H. C., Giavalisco, M., Mobasher, B., Grogin, N. A., & Panagia, N. 2007b, ApJ, submitted.
Williams, R. E., et al. 1996, AJ, 112, 1335
Willott, C. J., Rawlings, S., Jarvis, M. J., & Blundell, K. M. 2003, MNRAS, 339, 173
Wyithe, J. S. B., & Loeb, A. 2003, ApJ, 595, 614
Yan, H., et al. 2004, ApJ, 616, 63
Yan, H., Dickinson, M., Giavalisco, M., Stern, D., Eisenhardt, P. R. M., & Ferguson, H. C. 2006, ApJ, 651, 24
Yan, H., et al. 2005, ApJ, 634, 109
Yan, H., & Windhorst, R. A. 2004, ApJ, 612, L93
Yan, H., Windhorst, R. A., & Cohen, S. H. 2003, ApJ, 585, L93
York, D. G., et al. 2000, AJ, 120, 1579
Yoshida, N., Abel, T., Hernquist, L., & Sugiyama, N. 2003, ApJ, 592, 645
Yoshida, N., Omukai, K., Hernquist, L., & Abel, T. 2006, ApJ, 652, 6
Young, J. S., Schloerb, F. P., Kenney, J. D., & Lord, S. D. 1986, ApJ, 304, 443
Zamorani, G., et al. 1981, ApJ, 245, 357